batteries

MDPI

Review

All-Solid-State Anode-Free Sodium Batteries: Challenges and Prospects

Alexander M. Skundin * and Tatiana L. Kulova

A.N. Frumkin Institute of Physical Chemistry and Electrochemistry of the Russian Academy of Science, 119071 Moscow, Russia; tkulova@mail.ru
* Correspondence: askundin@mail.ru

Abstract

All-solid-state anode-free sodium batteries present a special and especially important kind of energy storage device. Unfortunately, the industrial production of such batteries has been absent up to now, although the prospects of their development seem to be rather optimistic. The present mini review considers the fundamental advantages of all-solid-state anode-free sodium batteries as well as challenges in their creation. The advantages of all-solid-state anode-free sodium batteries reveal themselves when comparing them with ordinary sodium-ion batteries, sodium metal batteries, sodium batteries with liquid electrolyte, and their lithium counterparts.

Keywords: anode-free batteries; sodium batteries; all-solid-state batteries; solid electrolytes; current constriction; sodium deposition

Academic Editor: Yong-Joon Park

Received: 4 July 2025
Revised: 25 July 2025
Accepted: 28 July 2025
Published: 2 August 2025

Citation: Skundin, A.M.; Kulova, T.L. All-Solid-State Anode-Free Sodium Batteries: Challenges and Prospects. *Batteries* **2025**, *11*, 292. https://doi.org/10.3390/batteries11080292

1. Introduction

So-called "anode-free" batteries are a specific but very promising kind of battery belonging to the post-lithium-ion era. Such batteries were first mentioned at the very end of the last century [1]. These were lithium metal batteries with solid electrolytes. Subsequently, various versions of anode-free lithium metal and sodium metal batteries with both solid and liquid electrolytes appeared. Surely, these batteries have two electrodes, and during discharge, one of them is the cathode and the other is the anode. Anode-free batteries are manufactured in a completely discharged state, and the negative electrode consists only of a current collector without active mass. During the first charge, lithium or sodium is deposited on this current collector at the expense of ions contained in the active material of the positive electrode. In the literature, one can find various synonyms for the term "anode-free battery", such as "anode-less battery", "zero-excess Li-metal battery", "reservoir-free battery", and so on.

The absence of active material on the negative electrode of a freshly assembled battery ensures a certain reduction in its weight and volume, i.e., an increase in energy density. An even more important advantage of anode-free sodium batteries over usual sodium metal ones is the significant simplification and reduction in cost of their production technology (at the assembly stage).

Unlike conventional batteries, the "electrolyte/negative electrode current collector" interface is of great importance for anode-free batteries, along with the "electrolyte/positive electrode active material" and "electrolyte/negative electrode active material" interfaces. There is currently extensive literature on anode-free lithium and sodium batteries with liquid electrolytes and on anode-free lithium batteries with solid electrolytes. Studies on the

development of anode-free sodium batteries with solid electrolytes are still in their infancy. This very circumstance was the authors' main motivation for writing this mini review. At the same time, many of the problems of such batteries are also inherent in anode-free sodium batteries with liquid electrolytes [2–8] and anode-free lithium batteries with solid electrolytes [7,9–11], as well as conventional (non anode-free) sodium batteries with solid electrolytes [12–17]. For the most part, these problems are related to sodium deposition during charging in the form of dendrites and their encapsulation, i.e., deposition of a solid electrolyte interphase (SEI) film on them.

The deposition of dendrites forming upon cathodic sodium is known to be connected with different factors. Firstly, in anode-free sodium metal batteries (no matter with liquid or solid electrolytes), sodium metal deposits directly onto foreign material of the current collector. The nucleation process in this case needs a rather high activation energy; therefore, it is non-uniform what is favorable for the growth of separate whiskers. Secondly, the above-mentioned SEIs, as a rule, contain a significant amount of flaws, which results in non-uniform electric fields and uncontrolled dendritic growth. The dendrite growth inevitably results in the breakdown of the separators and ultimately results in the short circuit of the battery. Sodium is a rather strong reducer, and in the course of its cathode deposition, a fresh, very active surface is formed. It is on this active surface that a passive film (SEI) grows, and since sodium is deposited in the form of dendrites, in many cases, the film completely envelops individual sodium particles, preventing their electronic contact with the current collector (encapsulation phenomenon).

The interface effect between electrode and solid electrolyte materials is the most critical issue for modern all-solid-state sodium batteries (both anode-free and ordinary). An ideal (or, at least, proper) interface between electrolyte and electrodes should have good compatibility and suitable mechanical strength as well as high ionic conductivity. In other words, this interface must reveal good sodiophility. Unfortunately, the contact of sodium metal and solid electrolytes faces interrelated challenges such as sluggish charge transfer kinetics, high interfacial resistance, uneven potential, and localized current density distribution, ultimately accelerating dendrite development.

The solid electrolytes for anode-free and ordinary sodium batteries must have high ionic conductivity along with a sufficiently high transference number of sodium ions, low electronic conductivity, a wide electrochemical window, chemical and mechanical stability, good mechanical properties, facile preparation, and environmental friendliness.

The solution to these problems usually comes down to modifying the current collector, electrolytes, and cycling mode (protocol).

2. The Interface Between a Solid Electrolyte and a Current Collector

Electrochemical processes at the interface between the solid electrolyte and the negative electrode current collector occur in anode-free batteries not only at the first charge, but also at further cycling during normal battery operation. In principle, such processes can also occur in a conventional (non-anode-free) sodium battery with a solid electrolyte during full discharge (or overdischarge) of the battery, but this is more likely to be related to improper operation (abuse) and should be avoided. The negative electrode current collector in a sodium battery can be made of different materials, and it is important to note that, unlike anode-free lithium batteries, in sodium batteries, this current collector can be made of both copper and aluminum, since sodium does not form alloys with aluminum and is not inserted into it.

The processes at the interface of the current collector with a solid electrolyte differ to a certain extent from the processes at the interface of the current collector with a liquid electrolyte. In the latter case, the entire surface of the current collector wetted with elec-

trolytes is the contact surface. At the interface of the solid current collector with a solid electrolyte, contact is ensured only at individual points (spots), and the configuration of these spots may depend on the degree of compression of the electrolyte and the current collector (Figure 1).

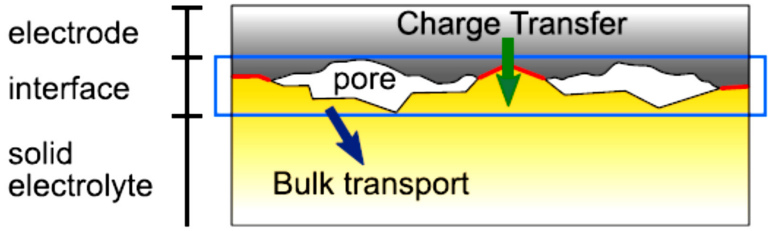

Figure 1. Schematic of the contact of the current collector (electrode) with a solid electrolyte. The contact surface on which charge transfer is possible is marked in red (from [18] open access).

A salient feature of such interfaces is the presence of voids (pores). As can be seen, the area of the electrochemically active surface is smaller than the total surface area, which leads to a certain decrease in the total current. This phenomenon, so-called current constriction, is well known in physics for contact between metals or semiconductors [19–21], but it has not been sufficiently studied in electrochemistry [18,22–25]. A natural consequence of current constriction is an increase in the total interfacial resistance [26,27], which also depends on the charge transfer resistance, the presence of SEI, and the presence of various contaminants. Of course, the picture shown in Figure 1 is not static, but it changes continuously when the current passes; the pore volume increases during the anodic dissolution of the metal and decreases during cathodic deposition. According to Faraday's laws, the passage of 1 Ah is accompanied by a change in the volume of sodium by 0.88 cm^3, which is 1.7 times greater than during the deposition/dissolution of lithium. In this regard, batteries with solid electrolytes compare favorably with batteries with liquid electrolytes, in which there is no free volume and the deposition of metallic sodium leads to the occurrence of internal stresses. Accordingly, the interfacial resistance increases in the anodic phase of cycling and decreases in the cathodic phase [24,25].

Some features of the interfaces of solid electrodes with a solid electrolyte associated with the occurrence of current constriction were studied using examples of different metals and different electrolytes. Thus, in [28–31], the interfaces of silver with AgI and AgBr and copper with CuBr, as well as platinum with CoO, were studied, and the occurrence of potential oscillations under galvanostatic conditions was discovered. The characteristic features of these oscillations depend on the current density, temperature, and compression force (pressure). Potential oscillations arise as a result of the periodic formation and disappearance of micropores and the corresponding changes in the contact surface area. Electrochemical dissolution occurs mainly at the points of dislocation exit to the surface, and it is in these places that micropores are formed. The walls of the micropores provide the rapid diffusion of metal adatoms.

Similar conclusions regarding the nature of current constriction were obtained in [32–34] using the example of lithium deposition from amorphous solid electrolyte LiPON (lithium phosphorus oxynitride) on substrates of different metals. In all cases, an increase in the current density of lithium deposition led to a decrease in the size of nuclei and to an increase in their number per unit surface area. The nucleation overpotential during lithium deposition on platinum (with which lithium forms an alloy) turned out to be significantly lower than the nucleation overpotential during lithium deposition on copper (when alloy formation is excluded). Potential oscillations were also observed during lithium deposition on platinum.

At the interface between copper and a crystalline lithium-conducting electrolyte with the garnet structure $Li_7La_3Zr_2O_{12}$ (LLZO), oscillations of even the open-circuit potential were observed, which, in turn, depended on the compression force [35] (Figure 2). An increase in the number of nuclei with increasing lithium deposition current density was also noted here, as well as preferential nucleation on surface defects [29,36].

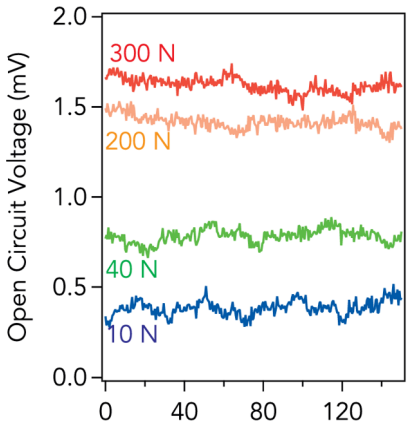

Figure 2. Oscillations of the open-circuit potential at the copper/LLZO interface under different compression forces (from [35] open access).

The most interesting and important aspect from this article's point of view is the work of [37], which studied the processes of sodium deposition and dissolution at the boundary of a copper current collector and a solid electrolyte NaSICON (Na SuperIonic CONductor). The electrolyte in this work had the composition $Na_{3.4}Zr_2Si_{2.4}P_{0.6}O_{12}$ (NZSP) (it should be noted that this is the electrolyte often used in studies of all-solid-state sodium-metal batteries [14,38–46]; one can find in the literature both notations "NaSICON" and "NASICON"). The processes of nucleation and deposit growth were studied at different current densities and different stack pressures using time-dependent impedance spectroscopy, confocal light microscopy, and electron microscopy. The studies were carried out using the electrochemical system Cu | NZSP | Na, where sodium served simultaneously as an auxiliary electrode and a reference one (quasi-reference electrode). The reliability of using such a reference electrode was confirmed in [38]. The galvanostatic curves of sodium deposition had an usual appearance, with a sharp shift of the potential to the negative direction at the moment of switching on the current, corresponding to the nucleation overpotential, and a subsequent gradual shift of the potential to the positive direction until reaching a steady-state value, corresponding to the current density [32,47,48]. Intriguingly, in this stationary section of the galvanostatic curve, sporadic fluctuations were recorded, the amplitude of which decreased somewhat with an increase in current density and stack pressure. Potential fluctuations were caused by local delamination of the copper current collector from the solid electrolyte and the corresponding increase in interphase resistance.

It is interesting that the nucleation overvoltage at a constant stack pressure was practically independent on the current density, but at a constant current density, it increased linearly with the increase in stack pressure (Figure 3). The latter fact is most intriguing, and it could be associated with a change in the pattern of contact between the electrode and the electrolyte (Figure 1). It should be emphasized here that it is the overvoltage of the nucleation stage that is considered, and not the deposit growth in the steady state (in the latter case, the overvoltage increases with increasing current density [37]). It is important to note that the influence of the stack pressure on the processes at the boundary of the current collector with the solid electrolyte has a clear physical nature. Some effects described for

the boundary of the current collector with the liquid electrolyte [49,50] more likely than not are some artifacts.

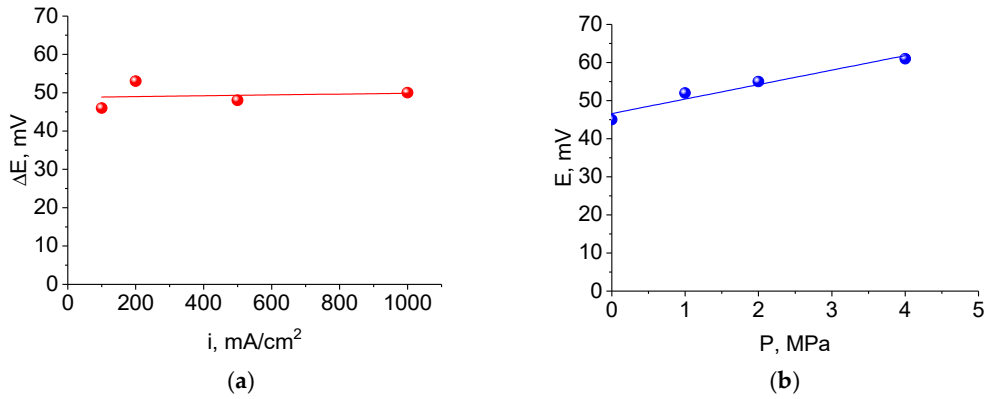

Figure 3. Dependence of nucleation overpotential on current density at a constant stack pressure of 2 MPa (**a**) and on stack pressure at a constant current density of 0.2 A/cm^2 (**b**) (constructed according to data from [37]).

At the same time, an increase in the current density was found to result in the formation of more uniform sodium deposits. Surprisingly, in this work, a practical absence of the effect of stack pressure on the morphology of sodium deposits was found; although, for lithium deposition under similar conditions, this effect is very noticeable [35,51]. This difference in the nature of lithium and sodium deposition is explained by the higher plasticity of sodium (the yield strength for lithium is 16 MPa [52], while for sodium it is only 0.2 MPa [53]).

In [36], the processes of sodium deposition and dissolution at the interface of a current collector made of aluminum with a carbon black coating and NZSP as an electrolyte were studied using electron backscatter diffraction (EBSD). It was found that sodium under these conditions was deposited in the form of fairly large crystallites (up to 150 μm wide), with the intercrystallite boundaries being strictly perpendicular to the plane of the current collector. During anodic dissolution of these deposits, voids (pores) were formed, and the interfacial resistance increased sharply.

To reduce the interfacial resistance at the interface between the solid electrolyte $Na_3Zr_2Si_2PO_{12}$ (NZSP(it is worth noting that the abbreviation NZSP is used for all stoichiometry of the compounds $Na_xZr_2Si_yP_zO_{12}$, and proper values of indexes x, y, z must be clear from context)) and the aluminum current collector, the work [54] proposes introducing an intermediate elastic ferroelectric layer with a thickness of about 3 μm, containing nanoparticles of barium titanate and carbon. Such a layer on the one hand dampens volumetric changes during the deposition and dissolution of sodium, and on the other hand, it makes the sodium ion flows more uniform. Accordingly, the sodium deposition is not in the form of dendrites but in the form of a smooth layer. In addition, the presence of this layer leads to a noticeable decrease in the nucleation overvoltage (from 53 to 4 mV at a current density of 0.1 mA/cm^2, and from 73 to 14 mV at a current density of 1 mA/cm^2). A laboratory model of an anode-free battery with the described intermediate layer, NZSP as an electrolyte, and a positive electrode based on $Na_3V_2(PO_4)_3$ (NVP) withstood 300 cycles with a current density of 0.1 mA/cm^2 with an insignificant loss of capacity (4.6%).

In [55,56], the initial stages of sodium whisker deposition at the interface of a gold current collector and polycrystalline Na-β″-alumina as an electrolyte were studied using the elegant method of in situ transmission electron microscopy (TEM) in combination with crystal orientation analysis (Figure 4). The sodium whiskers were found to grow along grain boundaries, and nucleation occurs not only directly at the interface of the electrolyte with gold, but also in the bulk of the electrolyte at the grain boundaries.

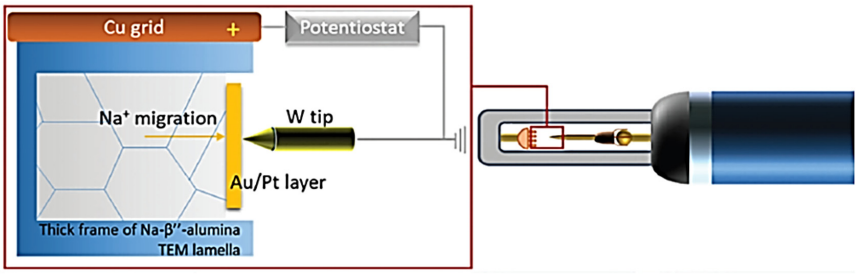

Figure 4. Schematic of the in situ transmission electron microscopy experiment used to study the deposition of sodium whiskers at grain boundaries (from [55] open access).

Thus, reducing the intergranular volume (in other words, increasing the relative density of the solid electrolyte) is an effective means of combatting dendrite formation.

3. The Interface Between a Solid Electrolyte and Sodium

In anode-free sodium batteries, the interface "solid electrolyte/sodium" appears just after the start of charging a freshly assembled or completely discharged battery. Naturally, such a boundary is also present in conventional (not anode-free) sodium metal batteries, and in the literature, one can find a lot of works on the study of such a boundary (see, for example, the review [57]). Of course, the fundamental issue is the compatibility of the solid electrolyte and sodium [43,58]. The interface "solid electrolyte/sodium" has many features of the interface "solid electrolyte/current collector", including the presence of voids and contact spots and, in general, the phenomenon of current constriction and, accordingly, increased interphase resistance. A significant problem is the risk of sodium deposition in the form of dendrites or whiskers, and the solution to this problem is associated with the modification of the solid electrolyte/sodium interface. It is the presence of voids and contact spots at such an interface that leads to uneven current density distribution and promotes the formation of dendrites [27,45,59]. It is worth noting that, since sodium has higher plasticity and a higher self-diffusion coefficient, the risk of dendrite formation at the solid electrolyte/sodium interface is less than at the solid electrolyte/lithium interface [60].

The penetration of sodium dendrites into a solid electrolyte depends on the presence of intercrystalline pores, i.e., on the deviation of the true density of the solid electrolyte from theoretical values, as well as on the ionic and electronic conductivity of the electrolyte (naturally, the former should be as large as possible, the latter as small as possible). In [61], it was shown that doping the solid electrolyte NASICON with ions of rare earth elements Pr^{3+}, Eu^{3+}, and Lu^{3+}, which have a larger radius than the replaced ion Zr^{4+}, leads to a noticeable increase in density, a decrease in electronic conductivity, and, accordingly, to a decrease in the risk of dendrite formation.

SEI on the sodium surface adjacent to a solid electrolyte compares favorably with SEI formed in a liquid electrolyte. In [39], the composition of SEI on a sodium electrode in a liquid electrolyte (1 M $NaClO_4$ in the mixture 95% propylene carbonate and 5% fluoroethylene carbonate) and in contact with a solid electrolyte (NASICON, $Na_3Zr_2Si_2PO_{12}$) was studied using time-of-flight secondary ion mass spectrometry (TOF-SIMS). Figure 5 shows the material distribution across the SEI thickness in both cases. In the SEI formed in the liquid electrolyte, the products of electrolyte decomposition (ions CH_2O^-, C_2F^-, NaO^-, and ClO_2^-) as well as the products transferred from the positive electrode (ions MnO^-, FeO^-, MnF_3^-, and FeF_3^-) were identified. In contact with the solid electrolyte, SEI was formed as a sodium oxide. It is important to emphasize that the SEI in contact with the solid electrolyte was much thinner than the SEI in the liquid electrolyte.

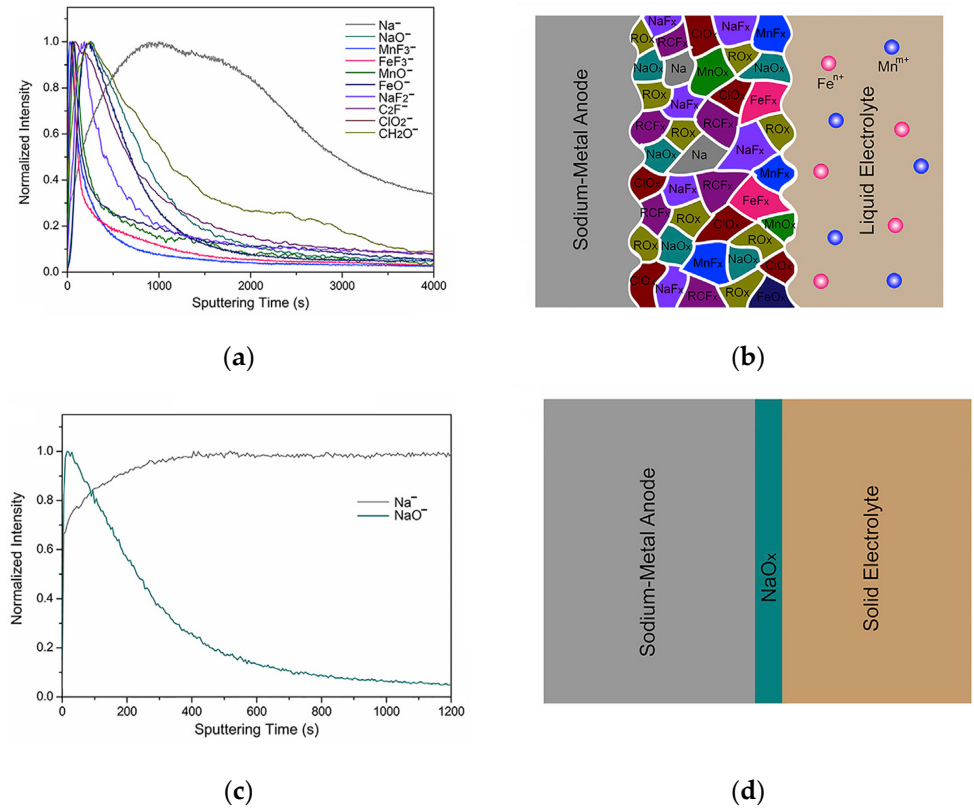

Figure 5. Distribution of SEI composition by depth for a liquid electrolyte (**a**,**b**) and solid electrolyte (**c**,**d**) (from [39] open access).

In [62] it is noted that natural SEIs at the sodium/NASICON interfaces have much higher protective properties than SEIs at the lithium/solid electrolyte interfaces.

High-quality SEI at the sodium/solid sulfide electrolyte ($Na_{2.895}W_{0.3}Sb_{0.7}S_4$) interface is obtained from a film of polyperfluoromethyl isopropyl ether $[CF(CF_3)CF_2O]_x(CF_2O)_y$. When in contact with sodium metal, this film is enriched by NaF and reliably prevents dendrite growth and reduces interfacial resistance [63].

Various strategies of modification of the solid electrolyte/sodium interface contribute to the improvement of the quality of this boundary, including the reduction of the interfacial resistance and the suppression of dendrite formation. Thus, in [40], it was shown that one of the reasons for the increased interfacial resistance at the NZSP-sodium interface is the presence of functional groups (in particular, hydroxyl and carbonate) on the NZSP surface. Annealing of NZSP in air at a temperature of 800 °C allows for cleaning the surface, and additional annealing at a temperature of 1000 °C leads to partial surface restoration and an increase in sodiophilicity and completely eliminates dendrite formation. It was found, in [41], that annealing of NZSP leads to the formation of a protective nanometric layer of Na_3PO_4. Annealing of NASICON to clean its surface from oxygen-containing groups is also recommended in [64]. In [65,66], it was shown that the tendency to form oxygen-containing functional groups on the NZSP surface depends on the annealing mode. Synthesis of NZSP in a two-stage mode (first stage 1300 °C, 15 min, second stage 1200 °C, 12 h) allows for it to reduce the number of surface groups, increase the ceramics density, and also increase its ionic conductivity.

A similar result is described in [67], where it is shown that surface treatment of NASICON with liquid sodium at a temperature of 380 °C leads to the formation of a reduced sodiophilic surface layer, which provides a tenfold decrease in interfacial resistance. In [14], it is proposed to treat the surface of NZSP with a suspension of SbF_3 in liquid sodium. With such treatment, the surface of the solid electrolyte is covered with a highly sodiophilic layer

of Na-Sb alloy containing NaF particles, which provide ionic conductivity. An original method for creating a sodiophilic surface of a solid electrolyte is described in [68]. Here, a porous layer of the same electrolyte about 0.1 mm thick is applied to the surface of a monolithic electrolyte (NZSP doped with Ca^{2+}). The porous layer is impregnated with a $SnCl_2$ solution and then annealed in air, converting all the tin into SnO_2. After this, the porous layer is impregnated with liquid sodium, whereby the pore walls are coated with metallic tin, and the entire porous layer acquires increased sodiophilicity.

A somewhat similar technique was used in [69]. Here, a thin SnO_2 layer was applied to the surface of a solid NASICON-like electrolyte of the composition $Na_{3.2}Hf_{1.9}Ca_{0.1}Si_2PO_{12}$. Upon contact with sodium metal, an intermediate Na_2O/Na_xSn layer was formed, which provided low interfacial resistance. To create a similar sodiophilic layer on the NASICON surface, the authors of [46] recommend applying a saturated aqueous solution of lead acetate to the surface and annealing in an argon atmosphere at a temperature of 550 °C. This creates a Pb/C@NZSP composite layer that is perfectly wetted by sodium. The interfacial resistance at the boundary of sodium with the solid electrolyte upon application of such a layer decreased from 391 to 1.5 Ohm·cm^2.

The authors of [70] proposed applying a suspension of Super P carbon black in a liquid Na–K alloy to the surface of a solid electrolyte $Na_3Hf_2Si_2PO_{12}$ (NHSP) to form a quasi-liquid composite layer C@Na-K with a thickness of about 7 μm (such a suspension has the properties of a non-Newtonian liquid).

In [71], it is proposed to apply a thin layer of AlF_3 to the NASICON surface (from an aqueous solution with subsequent drying and annealing at a temperature of 450 °C in a nitrogen atmosphere). This 350 nm thick AlF_3 layer evens out the unevenness of the NASICON surface and therefore reduces the tendency to dendrite formation and interfacial resistance. When such a modified NASICON comes into contact with metallic sodium, Al, NaF, and also $NamAlnF_3$ are formed. The resulting layer reliably prevents the deposition of sodium dendrites.

Another method for reducing the interfacial resistance at the solid electrolyte/sodium interface is by introducing a conducting polymer layer. In the already cited work [67], cross-linked poly (ethylene glycol) methyl ether acrylate (CPMEA) is proposed as such a polymer. In [72], a similar layer with a thickness of about 20 μm is made of a nanoporous product of copolymerization of 5,5′,6,6′-tetrahydroxy-3,3,3′,3′-tetramethyl-1,1′-spirobisindane and tetrafluoroterephthalo-nitrile, the molecular structure of which is shown in Figure 6.

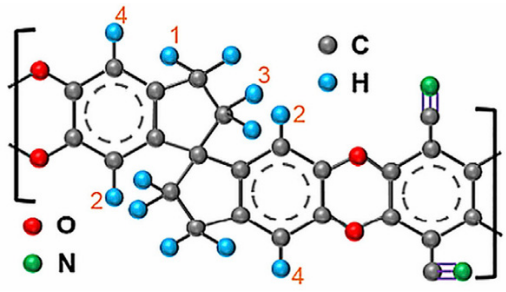

Figure 6. Molecular structure of the copolymerization product of 5,5′,6,6′-tetrahydroxy-3,3,3′,3′-tetramethyl-1,1′-spirobisindane and tetrafluoroterephthalonitrile (from [72] open access).

A sodiophilic interlayer made of sulfurized polyacrylonitrile (sulfurized PAN) on the surface of NASICON is proposed in [73].

In addition to polymers, the sodiophilic interlayer can be made simply of metals, in particular tin [74], oxides, e.g., TiO_2 [75], or carbon materials, specifically nanotubes [76] or graphene [77].

A relatively simple way to reduce the interfacial resistance at the solid electrolyte/sodium interface is proposed in [78]. It is shown here that doping $Na_3Zr_2Si_2PO_{12}$ with Zn^{2+} ions (replacing part of Zr with Zn) results in an increase in the electrolyte conductivity and, most importantly, in a decrease in the interfacial resistance. The electrolyte of the composition $Na_{3.20}Zr_{1.90}Zn_{0.1}0Si_2PO_{12}$ has a specific conductivity of 1.58 mS/cm, which is four times greater than that of the undoped electrolyte, and the interfacial resistance at the boundary with sodium for such an electrolyte was 25 Ohm·cm^2, whereas, for the undoped electrolyte, this resistance was 785 Ohm·cm^2. It was shown that zinc segregates on the surface of the solid electrolyte, where a layer of sodium-zinc alloy is formed, ensuring the sodiophilicity of the interface. The beneficial effect of doping the NASICON electrolyte with zinc was also reported in [79].

An even simpler way to reduce the interfacial resistance at the solid electrolyte/sodium interface is described in [80]. It is shown here that ultrasonic treatment of such an interface at room temperature for only 25 s (practically ultrasonic welding) results in the formation of a very close contact between sodium and the solid electrolyte NASICON ($Na_3Zr_2Si_2PO_{12}$) (Figure 7).

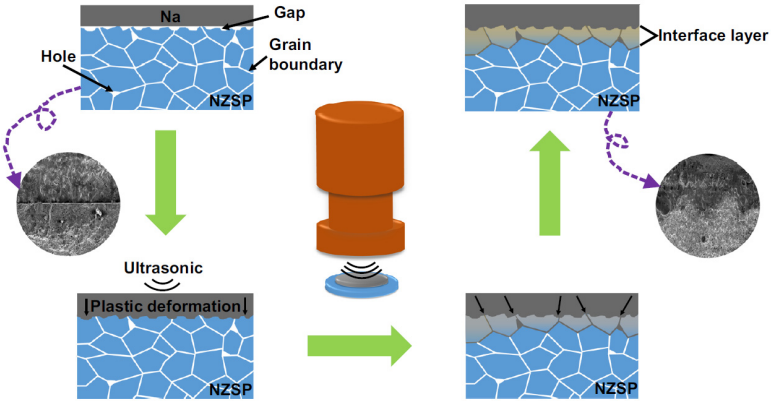

Figure 7. Schematic illustration of the ultrasound solid welding method (from [80] open access).

A symmetrical Na | $Na_3Zr_2Si_2PO_{12}$ | Na cell assembled using such ultrasound solid welding successfully withstood more than 200 cycles at a current density of 0.1 mA/cm^2 (1300 h) without any signs of dendrite formation or increase in overvoltage, which remained equal to 12 mV. A similar cell assembled without ultrasound solid welding did not withstand even 20 cycles.

The effect of stack pressure on the interfacial resistance at the solid electrolyte/current collector interface has already been noted above. Indicative data on the effect of uniaxial compression on the resistance at the solid electrolyte/sodium interface are presented in the study [81]. Here, the resistance of a NASICON pellet sandwiched between two sodium plates was measured at different compression pressures. The results are shown in Figure 8.

One can see that even a not too large compression pressure results in a decrease in interface resistance by an order of magnitude.

In the end of this section, it stands to right mentioning Refs. [82,83]. By using the density functional theory (DFT), it is shown here that monolayer coatings from some chalcogenides, namely $ScTe_2$ and V_2S_2, demonstrate the excellent sodiophilic properties.

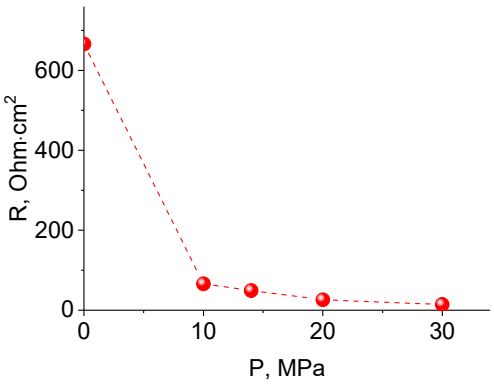

Figure 8. Dependence of interfacial resistance (R) at the NASICON/Na interface on the compression pressure (P) (constructed according to data from [81]).

4. The Interface Between a Solid Electrolyte and a Cathode

The interface between solid electrolyte and positive electrode in anode-free sodium batteries differs both from the interface between a solid electrolyte and negative electrode in such batteries and from the interface between a solid electrolyte and positive electrode in batteries with liquid electrolytes (although, of course, the interface between a solid electrolyte and cathode in anode-less sodium batteries is no different from the same interface in conventional, non-anode-free batteries). First of all, it is worth noting that there is a wide variety of possible active materials for positive electrodes. In addition to the most popular sodium vanadate-phosphate $Na_3V_2(PO_4)_3$ [80,84–89], the following oxides can be named: Na_xCoO_2 [90], $NaCrO_2$ [91], $NaNi_{0.4}Fe_{0.2}Mn_{0.4}O_2$ (NFM) [92], $Na_{0.66}Ni_{0.33}Mn_{0.67}O_2$ [93], P2–$Na_{0.68}Li_{0.10}Ni_{0.25}Mn_{0.63}Ca_{0.01}Ti_{0.01}O_2$ (NM-L10CN) [94], sodium titanophosphate $NaTi_2(PO_4)_3$ [67], double-cyano-perovskite $Na_2MnFe(CN)_6$ [39], perylene-3,4,9,10-tetracarboxylic dianhydride (PTCDA) [95], and pyrene-4,5,9,10-tetraone (PTO) [78].

Unlike the negative electrode, the positive one (cathode during discharge) contains a porous (essentially granular) active layer of a certain thickness. In order for such a layer to be able to operate across its entire thickness, it consists of a mixture of active material particles and a solid electrolyte, with the volume of solid electrolyte particles exceeding the percolation threshold to maintain the connectivity of all these particles. It is worth recalling that a certain amount of conductive additive, often carbon black, is also introduced into the active mass of the positive electrode to ensure electronic conductivity across the entire depth of the active layer. In addition, the actual particles of the active material are often coated with a nanometer layer of carbon. For example, in work [88], the active mass of the positive electrode included active material ($Na_3V_2(PO_4)_3$ with a carbon coating), a solid electrolyte ($Na_{3.4}Zr_{1.8}Mg_{0.2}Si_2PO_{12}$), a conductive additive (super P), and binder (PVDF—polyvinylidene fluoride) in a weight ratio of 65:20:5:10.

If the liquid electrolyte permeates the entire porous space and enables the entire internal surface to participate in the current-producing process, then the mixture of particles of the active material and the solid electrolyte provides only point-to-point contacts. A more elegant method of organizing good contact between the active material and the electrolyte is to coat each particle of the active material with the electrolyte, for example, using pulse laser deposition.

As in the case of the negative electrode, cycling (sodium insertion/extraction) of the positive electrode is accompanied by volume changes, however, they are generally smaller than that at the negative electrode. Thus, when extracting two sodium ions from $Na_3V_2(PO_4)_3$ (during charging), the volume decrease is only 0.21 cm^3/Ah, i.e., four times less than the change in the volume of sodium (with due account for the density of

$Na_3V_2(PO_4)_3$ equal to 3.156 g/cm^3 [87,96]). A significant difference between the interfaces of the solid electrolyte with the negative and positive electrodes also consists of the fact that, in the former case, the volume changes are one-dimensional and directed normally to the substrate surface, while, in the latter case, there is a three-dimensional change in the volume of each particle (granule) of the active material.

To improve the contact of the cathode material with the solid electrolyte (in essence, to reduce the interfacial resistance), in [85], it was proposed to wet the contact area of the NASICON solid electrolyte with the positive electrode based on sodium vanadate phosphate with a very small amount (0.5 μL/cm^2) of liquid electrolyte (0.8 M $NaPF_6$ in a mixture of ethylene carbonate with dimethyl carbonate) (Figure 9). This approach allowed them to significantly improve the battery characteristics, but due to partial evaporation and decomposition of the electrolyte, the cyclic resource was limited. A noticeable improvement was achieved by replacing the carbonate electrolyte with the same amount of ionic liquid (N-methyl-N-propylpiperidinium-bis(fluorosulfonyl) imide (PP13FSI)). In this version, the battery withstood 10,000 full charge–discharge cycles in the 10 C rate.

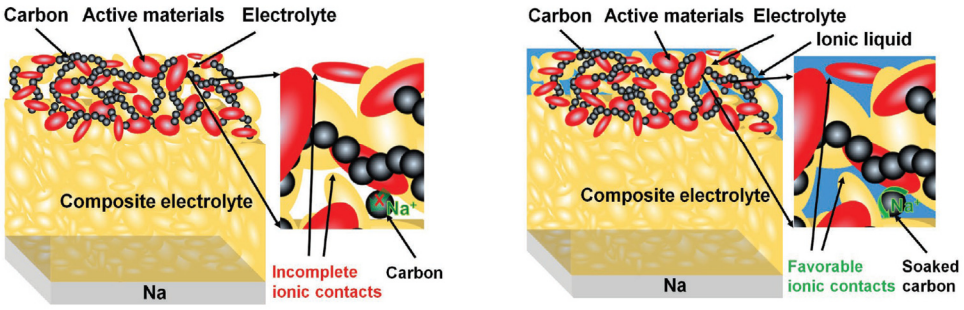

Figure 9. Contact of the cathode material with a solid electrolyte without (**a**) and with (**b**) wetting with a liquid electrolyte (from [85] with permission of Wiley).

A similar approach was used in [93]. Here, the active mass of the positive electrode is a paste (in the authors' terminology, "toothpaste") of $Na_{0.66}Ni_{0.33}Mn_{0.67}O_2$ particles with a carbon coating and *N*-butyl-*N*-methylpyrrolidinium bis(fluorosulfonyl)imide (PY14FSI) ionic liquid, the structural formula of which is shown in Figure 10. This paste is simply applied to the surface of Na-β″-Al_2O_3 solid electrolyte using a doctor blade.

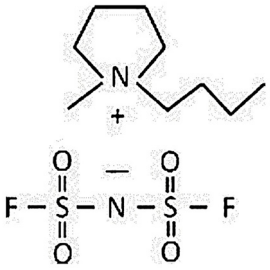

Figure 10. Structural formula of ionic liquid PY14FSI.

The authors of [84] proposed impregnating the active mass of the positive electrode with a so-called plastic–crystal Na+-electrolyte. This electrolyte is a complex obtained by heating a mixture of succinonitrile ($N{\equiv}C(CH_2)_2C{\equiv}N$) and $NaClO_4$ with a molar ratio of 20:1 at 65 °C. When cooled to room temperature, it solidifies, remaining X-ray amorphous, and it has an ionic conductivity of 3.3 mS/cm, which exceeds the conductivity of the lithium analogue [97].

As already mentioned above, the authors of [67] proposed a CPMEA polymer interlayer to reduce the interfacial resistance at the solid electrolyte/sodium interface. The same work proposes the same interlayer to reduce the interfacial resistance at the solid electrolyte/cathode interface. In this case, the cathode was made of sodium fluorotitanate using CPMEA as a binder that also has the properties of an ionic electrolyte.

Another polymer, namely a copolymer of vinylidene fluoride with hexafluoropropylene (PVDF–HFP) for the same purposes, is proposed in [92]. Here, a mixture of PVDF–HFP with a suspension of the active material NFM in N-methylpyrrolidone was applied directly to the surface of the solid electrolyte ($Na_3Zr_2Si_{2.2}P_{0.8}O_{12}$).

In [94], a very sophisticated active material of the positive electrode, specifically $Na_{0.68}Li_{0.10}Ni_{0.25}Mn_{0.63}Ca_{0.01}Ti_{0.01}O_2$ (NM-L10CN), was reported. A battery with such an electrode and solid NZSP electrolyte, successfully withstood 500 cycles at 1 C rate. Intriguingly, this article says nothing about measures to reduce interphase resistance at the boundary of the solid electrolyte with the cathode.

It is known that materials such as Prussian blue, although attractive in terms of specific capacity, are unstable in contact with liquid organic electrolytes. In the above-mentioned work [39], the performance of such material, specifically double-cyano-perovskite with formula $Na_2MnFe(CN)_6$ (NMHCF), was assessed in contact with the $Na_3Zr_2Si_2PO_{12}$ solid electrolyte. The active mass of the positive electrode in this case was made from a mixture of NMHCF, carbon black as an electrically conductive additive, and a solid polymer electrolyte based on polyethylene oxide and $NaClO_4$. Such a battery successfully withstood 200 cycles at the C/2 rate with a loss of only 10% of capacity.

5. Solid Electrolytes

In principle, the solid electrolyte for an anode-free sodium battery is no different from the solid electrolyte for a conventional (not-anode-free) battery. This explains the fact that there are a huge number of publications in the literature on solid electrolytes for conventional sodium batteries (it is high time to mention review papers such as [13,15,43,98–107]) but practically nothing on anode-free versions. Indeed, we are unaware of research devoted to this very topic. The main requirements for solid electrolytes for anode-free sodium batteries are obvious. Such electrolytes must possess sufficiently high conductivity for sodium ions and a sufficiently high transference number of such ions, a wide electrochemical stability window, chemical and mechanical stability, low electronic conductivity, ability to inhibit dendrites, good mechanical properties, facile preparation, and environmental friendliness. Of particular importance is the requirement for a high sodium ion transference number, since a deviation of this quantity from unity leads to the occurrence of concentration polarization with a corresponding decrease in discharge voltage and energy density.

Solid polymer electrolytes are sometimes included in the category of solid electrolytes, but polymers should be considered supercooled liquids rather than true solids. In addition, solid polymer electrolytes, as a rule, possess rather low sodium ion transference numbers. They are not considered in this article. Among the numerous inorganic solid electrolytes with sodium conductivity, groups such as NASICON-type materials, sulfides [108], and complex hydrides [100,108] can be distinguished. The most popular are NASICON-type materials, which were proposed as an electrolyte in 1976 as an alternative to β-alumina [109,110].

The composition of NASICON-type material can be described by the generalized formula $NaMM'(PO_4)_3$, where the M and M′ positions can contain various transition metal ions in the divalent, trivalent, tetravalent, or pentavalent states, and phosphorus can be partially replaced by silicon or arsenic [105]. Standard ceramic methods are used to synthesize NASICON-like electrolytes, i.e., sintering of precursor's mixtures, which are obtained

by simple dry mixing, sol-gel route, hydrothermal method, or ion exchange. Depending on the composition and synthesis method, NASICON can crystallize in the following structures: a rhombohedral (prevalent in NASICON system), monoclinic, triclinic, orthorhombic, corundum-like, etc. NASICON-like electrolytes have a specific ionic conductivity of about 0.1 mS/cm at room temperature, which depends on the specific composition and crystal structure [111]. For example, in [112], it was found that the introduction of a superstoichiometric amount of sodium into standard NASICON (transition from $Na_3Zr_2Si_2PO_{12}$ to $Na_{3.3}Zr_2Si_2PO_{12}$) leads to an increase in the room-temperature specific conductivity from 0.2 to 0.9 mS/cm. A similar result (2.4 mS/cm for $Na_{3.3}Zr_2Si_2PO_{12}$) was reported in [113]. In [114], materials of the compositions $Na_{3.4}Zr_2Si_{2.5}P_{0.5}O_{12}$ and $Na_{3.4}Zr_2Si_{2.4}P_{0.6}O_{12}$ with a specific conductivity of about 5 mS/cm were reported.

In [115], it was shown that doping NASICON with yttrium (by replacing the ZrO_2 precursor with $(ZrO_2)_{0.97}(Y_2O_3)_{0.03}$) leads to a fivefold increase in ionic conductivity. In general, doping with cations is an effective means of increasing the ionic conductivity of NASICON [106,116–121], with hafnium, yttrium, niobium, cobalt, and zinc being the most effective dopants. Among the NASICON-like materials with the highest ionic conductivity at room temperature, the following should be mentioned: $Na_{3.2}Hf_2(SiO_4)_{2.2}(PO_4)_{0.8}$ (specific conductivity 2.3 mS/cm) [122], $Na_{3.4}Zr_{1.8}Ni_{0.2}Si_2PO_{12}$ (2.28 mS/cm) [116], $Na_{3.3}Hf_2(SiO_4)_2(PO_4)$ (1.1 mS/cm) [122], $Na_{3.36}Zn_{0.08}Zr_{1.92}(SiO_4)_{2.2}(PO_4)_{0.8}$ (1.1 mS/cm) [123], $Na_3Zr_{1.8}Zn_{0.2}Si_2PO_{11.8}$ (1.44 mS/cm) [120], $Na_{3.232}Co_{0.016}Zr_{1.984}(SiO_4)_{2.2}(PO_4)_{0.8}$ (1.41 mS/cm) [124], $Na_{2.1}Y_{0.1}Zr_{1.9}(SiO_4)_2(PO_4)$ (1.98 mS/cm) [117], $Na_{3.5}Zr_{1.75}Mg_{0.25}Si_2O_{12}$ (2.5 mS/cm) [113], $Na_{3.4}Sc_{0.4}Zr_{1.6}(SiO_4)_2(PO_4)$ (4.0 mS/cm) [125], $Na_{2.96}Nb_{0.04}Zr_{1.96}(SiO_4)_2(PO_4)$ (4.95 mS/cm) [117], and $Na_{3.4}Zr_{1.9}Zn_{0.1}Si_{2.2}P_{0.8}O_{12}$ (5.27 mS/cm) [121].

As was indicated in Section 2, a decrease in the intergranular volume (an increase in the relative density of NASICON) is important from the point of view of combatting dendrite formation. Doping NASICON with cations in some cases leads to a noticeable increase in the relative density [68,85,121,126]. In [61], it was shown that large ions of rare earth elements such as Pr^{3+}, Eu^{3+}, and Lu^{3+} are particularly effective in this regard. Thus, if the relative density of undoped $Na_3Zr_2Si_2PO_{12}$ is 87.8%, then for $Na_{3.3}Zr_{1.7}Pr_{0.3}Si_2PO_{12}$, $Na_{3.3}Zr_{1.7}Eu_{0.3}Si_2PO_{12}$, and $Na_{3.3}Zr_{1.7}Lu_{0.3}Si_2PO_{12}$, it increases to 94.2%, 94.5%, and 92.3%.

Besides doping, various technological methods are an important means of increasing ionic conductivity. For example, in [127], a NASICON-like electrolyte was synthesized by sintering a mixture of canonical $Na_3Zr_2Si_2PO_{12}$ with the addition of 5% Na_2SiO_3 at a temperature exceeding the melting point of Na_2SiO_3. The resulting material had an ionic conductivity at room temperature as high as 1.45 mS/cm, which was associated with the formation of a non-stoichiometrically silicon-enriched phase at the intercrystalline boundaries.

Sulfides are the second most important group of inorganic solid electrolytes with sodium ion conductivity [128]. The most important are electrolytes based on Na_3PS_4 [129], Na_3SbS_4 [130,131], and $Na_{11}Sn_2PS_{12}$ [132]. Sulfide electrolytes are characterized by a wide electrochemical stability window (over 5 V) and stability to sodium [133–136]. There are amorphous (glassy), crystalline, and glass-ceramic samples. Plain amorphous examples of the Na_2S–P_2S_5 system have rather modest ionic conductivity at room temperature (about 0.01 mS/cm). The transition to crystalline forms and to glass ceramics makes it possible to increase this conductivity to fractions of mS/cm [129,133,135,137–139]. An even greater increase in ionic conductivity can be achieved through doping, mainly anionic [140–146].

The positive effect of replacing part of the phosphorus in Na_3PS_4 with arsenic is described in [147]. The material with the composition $Na_3P_{0.62}As_{0.38}S_4$ has a room-temperature conductivity of about 1.46 mS/cm. The most effective cationic dopants are silicon, germanium, and tin. According to [145], the ionic conductivity at room temperature for materials with the compositions $Na_{3.125}Si_{0.125}P_{0.875}S_4$ and $Na_{3.0625}Sn_{0.0625}P_{0.9375}S_4$

amounts to 2.99 and 10.7 mS/cm. The ionic conductivity of $Na_{3.1}Ge_{0.1}Sb_{0.9}S_4$ at room temperature is 5.1 mS/cm [146].

In [142,144,148], it is shown that the substitution of sulfur in Na_3PS_4 with selenium leads to a noticeable increase in ionic conductivity. Thus, according to [144], Na_3PSe_4 has a specific conductivity of 1.16 mS/cm at room temperature. More importantly, the transference number for the Na^+ cation in Na_3PSe_4 is practically equal to unity.

Probably, the compound $Na_{2.88}Sb_{0.88}W_{0.12}S_4$ has the highest ionic conductivity among doped sulfides; the literature gives room-temperature ionic conductivity values of 2.5 [149], 19 [150], and 32 mS/cm [151]. This discrepancy is due to different heat treatment conditions of the ceramics; the value of 32 mS/cm was obtained after 12 h annealing at 275 °C, which resulted in higher crystallinity and density. Figures 11 and 12 compare the crystal structure of $Na_{2.88}Sb_{0.88}W_{0.12}S_4$ and undoped Na_3SbS_4. The inclusion of tungsten in crystalline Na_3SbS_4 results in the appearance of Na vacancies in the lattice, which promotes the formation of a cubic phase, which can facilitate isotropic three-dimensional conductivity of fast ions.

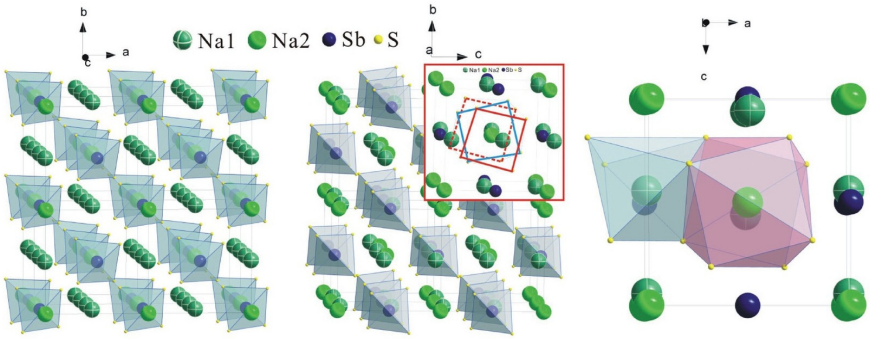

Figure 11. The crystal structure of Na_3SbS_4 viewed along the c (left panel) and a axes (middle panel), and Na1 and Na2 coordination environments (right panel). The inset of the middle panel illustrates diffusion channels along the a-direction composed by S-anion distorted cubic sublattices (from [130] open access).

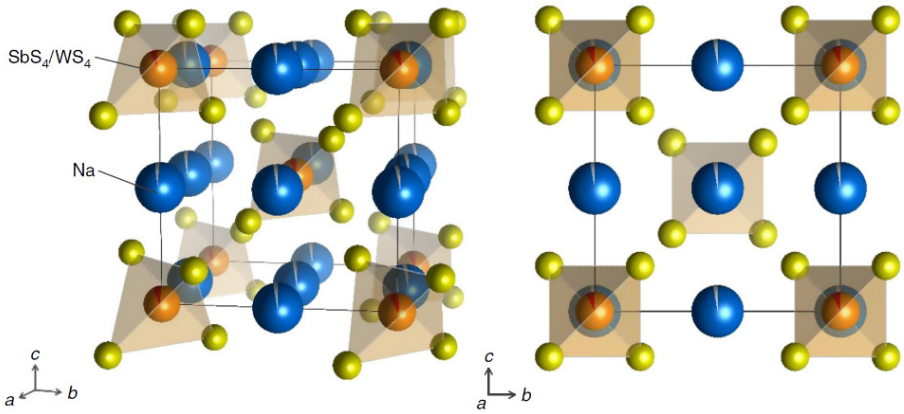

Figure 12. Crystal structure of cubic $Na_{2.88}Sb_{0.88}W_{0.12}S_4$ with the unit cell outlined. The Na, Sb, W, and S sites are represented by blue, orange, gray, and yellow balls, respectively. Na is linearly arranged, and distortion of the SbS_4/WS_4 tetrahedra is very small compared to the tetragonal structure of Na_3SbS_4 (from [151] open access).

The transference number of the Na^+ cation in this case was also close to unity. Interestingly, the $Na_{2.88}Sb_{0.88}W_{0.12}S_4$ composites with sodium iodide have an even higher ionic conductivity, which depends on the NaI content. The maximum conductivity of 36 mS/cm is exhibited by the $Na_{2.88}Sb_{0.88}W_{0.12}S_4 \cdot 0.50NaI$ composite [149] (Figure 13). At the same

time, the introduction of NaI into the composite with Na_3PS_4 does not lead to a noticeable increase in conductivity [152].

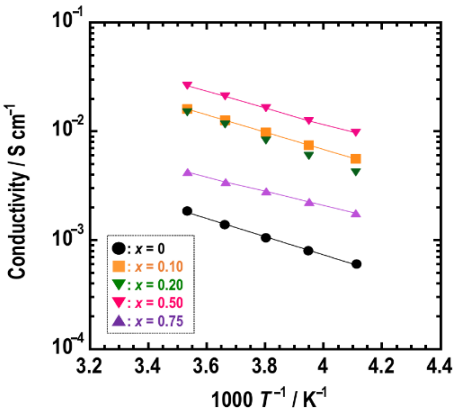

Figure 13. The effect of NaI upon conductivity of $Na_{2.88}Sb_{0.88}W_{0.12}S_4 \cdot x$NaI (from [149] open access).

The properties of the $Na_{3-x}P_{1-x}W_xS_4$ electrolyte depend on both the composition (degree of tungsten addition) and the synthesis method [153]. With the same mechanochemical synthesis, compositions with x = 0.09, 0.15, 0.18, and 0.21 had specific conductivities of 1.84, 8.8, 2.47, and 1.69 mS/cm, respectively. At the same time, according to data from [154], the $Na_{2.9}P_{0.9}W_{0.1}S_4$ electrolyte synthesized by solid-phase synthesis had a conductivity of 13 mS/cm, while $Na_{2.9}Sb_{0.9}W_{0.1}S_4$ had a conductivity of 41 mS/cm. It is worth noting that such properties of $Na_{11}Sn_2PS_{12}$ are not too sensitive to small changes in composition. According to [155], electrolytes with compositions $Na_{11}Sn_2PS_{12}$, $Na_{10.875}Sn_2PS_{12}$, and $Na_{11.125}Sn_2PS_{12}$ have conductivities of 2.4, 2.3, and 2.4 mS/cm, respectively. At the same time, the conductivity of $Na_{10}SnP_2S_{12}$ is only 0.4 mS/cm [156].

Important dopants for sulfide electrolytes are halides. Thus, in [140], it was shown that $Na_{2.9375}PS_{3.9375}Cl_{0.0625}$ has a conductivity of 1.38 mS/cm at room temperature. In a later work of the same team [157], for $Na_3PS_{3.8}Cl_{0.2}$, $Na_{2.875}PS_{3.875}Cl_{0.125}$, and $Na_{2.9375}PS_{3.875}Cl_{0.125}$, the ionic conductivity values of 1.6, 6.38, and 9.03 mS/cm are reported. In [158], a series of halogen-substituted sulfides of the general formula $Na_{3-x}SbS_{4-x}Hal_x$ ($0 \leq x \leq 0.3$, Hal = Cl, Br, and I) was studied, and it was found that $Na_{2.85}SbS_{3.85}Br_{0.15}$ has the maximum room-temperature ionic conductivity of 2.87 mS/cm.

Of interest is the effect of doping sulfide electrolytes with oxygen on their conductivity and stability in contact with sodium. The authors of [159] investigated the introduction of small amounts of phosphorus and oxygen (in a ratio of 4 P:10 O) into the Na_3SbS_4 glass ceramic electrolyte and found that the highest ionic conductivity of 3.82 mS/cm was possessed by the composition $Na_3SbP_{0.16}S_4O_{0.4}$, pre-annealed in a vacuum at a temperature of 500 °C for 10 h (annealing led to an increase in crystallinity). At the same time, in [150], it was discovered that the introduction of oxygen into $Na_{2.88}Sb_{0.88}W_{0.12}S_4$ due to the substitution of sulfur led to a slight decrease in ionic conductivity. Moreover, based on first-principle calculations in [160], it was shown that the ionic conductivity of $Na_7P_3O_{11}$ at room temperature is only 3 μS/cm, whereas for $Na_7P_3S_{11}$ and $Na_7P_3Se_{11}$, values of 10.97 and 12.56 mS/cm, respectively, were obtained.

Of other types of solid electrolytes, mention should be made of hydride (and borohydride) systems [161,162], thioborates [163], and the chloride electrolyte ($Na_{1-x}Zr_xLa_{1-x}Cl_4$) [164], although they are of much less importance than NASICON and sulfides.

6. Forecast of Possible Characteristics of Future All-Solid-State Anode-Free Sodium Batteries

As is clear from the Section 1, we are unaware of any literature data on the characteristics of specific all-solid-state anode-free sodium batteries. However, published data on the electrochemical properties of ordinary all-solid-state sodium battery systems provide an idea of the possible performance of future anode-free counterparts. Table 1 provides literature data on various electrochemical systems of all-solid-state sodium batteries.

Table 1. Comparison of the characteristics of all-solid-state sodium batteries based on different electrochemical systems.

Electrolyte	Cathode	Anode	Voltage Range, V	Ionic Conductivity of Electrolyte, RT, S/cm	Cathode Specific Capacity, mAh/g	Cycles	Ref.
$Na_3Zr_2Si_2PO_{12}$	$Na_2MnFe(CN)_6$	Na	4.0–2.5	$1.2{\cdot}10^{-3}$ at 60 °C	120 at 0.5 C	200	[39]
$Na_{3.4}Zr_2(SiO_4)_{2.4}(PO_4)_{0.6}$	$Na_3V_2(PO_4)_3$	Na	3.8–2.0	$5{\cdot}10^{-3}$	0.6 mAh/cm^2 at 0.5 mA/cm^2	70	[45]
$Na_3Zr_2Si_2PO_{12}$	$Na_3V_2(PO_4)_3$	Na	3.8–2.0	$6{\cdot}10^{-4}$	88 at 0.2 C	100	[46]
$Na_3Zr_2Si_2PO_{12}$	$NaCu_{1/9}Ni_{2/9}Fe_{1/3}Mn_{1/3}O_2$	$BaTiO_3$/C@Al	3.8–2.0	$6{\cdot}10^{-4}$	93.1 at 0.1 mA/cm^2	300	[54]
$Na_3Zr_2Si_2PO_{12}$	$Na_{3.5}V_{0.5}Mn_{0.5}Fe_{0.5}Ti_{0.5}(PO_4)_3$	Na	4.4–2.0	$6{\cdot}10^{-3}$	152 at 1 C	1000	[65]
$Na_3Zr_2Si_2PO_{12}$	$Na_3V_{1.5}Cr_{0.5}(PO_4)_3$	Na	4.3–2.5	$0.85{\cdot}10^{-3}$	103 at 1 C	400	[66]
$Na_{3.2}Zr_{1.9}Ca_{0.1}Si_2PO_{12}$	$Na_3V_2(PO_4)_3$	Na	3.8–2.7	$1.67{\cdot}10^{-3}$	94.9 at 1 C	450	[68]
$Na_{3.2}Hf_{1.9}Ca_{0.1}Si_2PO_{12}$	$Na_3V_2(PO_4)_3$	Na/SnO_2	3.8–2.7	$1.07{\cdot}10^{-3}$	103.1 at 0.5 C	300	[69]
β″-Al_2O_3	$Na_3V_2(PO_4)_3$	Na	3.8–2.5	$1.17{\cdot}10^{-4}$	100 at 0.2 C	100	[76]
$Na_3Zr_2Si_2PO_{12}$	$Na_3V_2(PO_4)_3$	Na	4.0–2.6	$4.3{\cdot}10^{-4}$	110 at 0.1 mA/cm^2	900	[80]
$Na_3Zr_2Si_2PO_{12}$	$Na_3V_2(PO_4)_3$	Na	4.0–2.5	$3.3{\cdot}10^{-4}$	90 at 0.1 C	100	[84]
$Na_{3.4}Zr_{1.6}Sc_{0.4}Si_2PO_{12}$	$Na_3V_2(PO_4)_3$	Na	3.8–2.3	$1.77{\cdot}10^{-4}$	100 at 1 C	300	[86]
Na-β″-Al_2O_3	$Na_{0.66}Ni_{0.33}Mn_{0.67}O_2$	Na	3.8–2.5	$1.0{\cdot}10^{-3}$	79 at 6 C	10,000	[93]
$Na_{3.4}Zr_{1.9}Zn_{0.1}Si_{2.2}P_{0.8}O_{12}$	FeS_2	Na	2.5–0.7	$5.27{\cdot}10^{-3}$	236.5 at 0.1 C 133.1 at 0.5 C	100 300	[121]
$Na_{3.1}Zr_{1.95}Mg_{0.05}Si_2PO_{12}$	$Na_{0.9}Cu_{0.22}Fe_{0.3}Mn_{0.48}O_2$	Na	3.8–2.5	$1.33{\cdot}10^{-3}$	57.9 at 0.5 C	100	[126]
Na_3PS_4	$NaCrO_2$	$Na_{15}Sn_4$	4.0–1.0	$4.6{\cdot}10^{-4}$	90 at 0.013 mA/cm^2	20	[129]
Na_3PS_4	$NaCrO_2$	$Na_{15}Sn_4$	3.0–1.0	$4.0{\cdot}10^{-4}$	250	10	[131]
Na_3SbS_4	$NaCrO_2$	Na	4.0–1.5	$1.1{\cdot}10^{-3}$	108 at 0.05 mA/cm^2	1	[134]
t-$Na_{2.9375}PS_{3.9375}Cl_{0.0625}$	TiS_2	Na	2.4–1.2	$1.14{\cdot}10^{-3}$	80 at 0.1 C	10	[140]
$Na_3P_{0.62}As_{0.38}S_4$	TiS_2	Na-Sn	2.4–1.2	$1.46{\cdot}10^{-3}$	150 at 0.02 C	10	[147]
$Na_{2.88}Sb_{0.88}W_{0.12}S_4{\cdot}0.5NaI$	TiS_2	Na-Sn	2.4–1.2	10^{-2}	100 at 0.057 C	5	[149]
$Na_{2.88}Sb_{0.88}W_{0.12}S_{3.7}O_{0.3}$	TiS_2	Na-Sn	2.4–1.2	$2.2{\cdot}10^{-3}$	130 at 0.057 C	5	[150]
$Na_{2.85}P_{0.85}W_{0.15}S_4$	TiS_2	Na-Sn	2.4–1.2	$8.8{\cdot}10^{-3}$	140 at 0.057 C	5	[153]
$Na_{3.0}PS_{3.8}Cl_{0.2}$	$Na_3V_2(PO_4)_3$	Na	3.8–2.5	$1.96{\cdot}10^{-3}$	100 at 0.1 C	10	[157]
$Na_{0.7}Zr_{0.3}La_{0.7}Cl_4$	$NaCrO_2$	Na_2Sn	3.4–2.0	$2.9{\cdot}10^{-4}$	114 at 0.3 C	70	[164]

7. Conclusions

All-solid-state anode-free sodium batteries present a special category of energy storage devices. Up to date, there are neither industrially produced batteries, nor laboratory ones like these such batteries, but the prospects for their creation are quite optimistic. This optimism is explained by the fundamental advantages of solid-state anode-free sodium batteries over other categories.

The advantages of anode-free sodium batteries over sodium-ion batteries are greater specific capacity and energy density. The advantages of anode-free sodium batteries over

conventional sodium metal batteries are the absence of operations with metallic sodium during production and assembly, that is, in the radical simplification and reduction of the cost of technology. The advantages of batteries with a solid electrolyte over batteries with a liquid electrolyte are greater chemical stability, good mechanical properties, and increased safety. In addition, solid electrolytes usually have a sodium cation transference number close to one, which ensures an increase in energy density. The advantages of solid-state anode-free sodium batteries over their lithium counterparts include the much lower cost and greater availability of sodium, as well as the ability to use aluminum rather than copper as a current collector.

The above-listed advantages of all-solid-state anode-free sodium batteries have certain economic and environmental aspects. The already mentioned simplification and reduction in cost of the production technology of such batteries, associated with the exclusion of operations with sodium metal, also contribute to a significant scaling of production, which is especially important for energy storage systems. The exclusion of liquid electrolytes provides certain environmental advantages both in the production and in the recovering of batteries.

Author Contributions: A.M.S.—conceptualization, analysis of literature, writing and editing of the original draft; T.L.K.—conceptualization, analysis of literature, writing of original draft. All authors have read and agreed to the published version of the manuscript.

Funding: This work was funded by Russian Science Foundation, grant number 25-13-00125. https://rscf.ru/en/project/25-13-00125/. Accessed on 30 May 2025.

Data Availability Statement: Not applicable.

Conflicts of Interest: The authors declare no conflicts of interest.

References

1. Neudecker, B.J.; Dudney, N.J.; Bates, J.B. "Lithium-Free" Thin-Film Battery with In Situ Plated Li Anode. *J. Electrochem. Soc.* **2000**, *147*, 517–523. [CrossRef]
2. Ni, Q.; Yang, Y.; Du, H.; Deng, H.; Lin, J.; Lin, L.; Yuan, M.; Sun, Z.; Sun, G. Anode-Free Rechargeable Sodium-Metal Batteries. *Batteries* **2022**, *8*, 272. [CrossRef]
3. Hu, Z.; Liu, L.; Wang, X.; Zheng, Q.; Han, C.; Li, W. Current Progress of Anode-Free Rechargeable Sodium Metal Batteries: Origin, Challenges, Strategies, and Perspectives. *Adv. Funct. Mater.* **2024**, *34*, 2313823. [CrossRef]
4. Chen, Y.; Ye, C.; Zhang, N.; Liu, J.; Li, H.; Davey, K.; Qiao, S. Prospects for practical anode-free sodium batteries. *Mater. Today* **2024**, *73*, 260–274. [CrossRef]
5. Yang, T.; Luo, D.; Liu, Y.; Aiping Yu, A.; Chen, Z. Anode-free sodium metal batteries as rising stars for lithium-ion alternatives. *iScience* **2023**, *26*, 105982. [CrossRef]
6. Xu, P.; Huang, F.; Sun, Y.; Lei, Y.; Cao, X.; Liang, S.; Fang, G. Anode-Free Alkali Metal Batteries: From Laboratory to Practicability. *Adv. Funct. Mater.* **2024**, *34*, 2406080. [CrossRef]
7. Tian, Y.; An, Y.; Wei, C.; Jiang, H.; Xiong, S.; Feng, J.; Qian, Y. Recently advances and perspectives of anode-free rechargeable batteries. *Nano Energy* **2020**, *78*, 105344. [CrossRef]
8. Li, Y.; Zhou, Q.; Weng, S.; Ding, F.; Qi, X.; Lu, J.; Li, Y.; Zhang, X.; Rong, X.; Lu, Y.; et al. Interfacial engineering to achieve an energy density of over 200 Wh kg^{-1} in sodium batteries. *Nat. Energy* **2022**, *7*, 511–519. [CrossRef]
9. Heubner, C.; Maletti, S.; Auer, H.; Hüttl, J.; Voigt, K.; Lohrberg, O.; Nikolowski, K.; Partsch, M.; Michaelis, A. From Lithium-Metal toward Anode-Free Solid-State Batteries: Current Developments, Issues, and Challenges. *Adv. Funct. Mater.* **2021**, *31*, 2106608. [CrossRef]
10. Xie, Z.; Wu, Z.; An, X.; Yue, X.; Wang, J.; Abudula, A.; Guan, G. Anode-free rechargeable lithium metal batteries: Progress and prospects. *Energy Storage Mater.* **2020**, *32*, 386–401. [CrossRef]
11. Tong, Z.; Bazri, B.; Hu, S.; Liu, R.S. Interfacial chemistry in anode-free batteries: Challenges and strategies. *J. Mater. Chem. A* **2021**, *9*, 7396–7406. [CrossRef]
12. Zhao, C.; Liu, L.; Qi, X.; Lu, Y.; Wu, F.; Zhao, J.; Yu, Y.; Hu, Y.; Chen, L. Solid-State Sodium Batteries. *Adv. Energy Mater.* **2018**, *8*, 1703012. [CrossRef]

13. Fan, L.; Wei, S.; Li, S.; Li, Q.; Lu, Y. Recent Progress of the Solid-State Electrolytes for High-Energy Metal-Based Batteries. *Adv. Energy Mater.* **2018**, *8*, 1702657. [CrossRef]
14. Lu, G.; Li, M.; Deng, R.; Hou, W.; Lu, L.; Song, S.; Xu, C.; Wang, R. Ultralong lifespan solid-state sodium battery with a supersodiophilic and fast ionic conductive composite sodium anode. *Energy Storage Mater.* **2024**, *72*, 103755. [CrossRef]
15. Janek, J.; Zeier, W.G. Challenges in speeding up solid-state battery development. *Nat. Energy* **2023**, *8*, 230–240. [CrossRef]
16. Zheng, X.; Bommier, C.; Luo, W.; Jiang, L.; Hao, Y.; Huang, Y. Sodium Metal Anodes for Room-Temperature Sodium-Ion Batteries: Applications, Challenges and Solutions. *Energy Storage Mater.* **2019**, *16*, 6–23. [CrossRef]
17. Zhao, Y.; Adair, K.R.; Sun, X. Recent developments and insights into the understanding of Na metal anodes for Na-metal batteries. *Energy Environ. Sci.* **2018**, *11*, 2673–2695. [CrossRef]
18. Eckhardt, J.K.; Klar, P.J.; Janek, J.; Heiliger, C. Interplay of Dynamic Constriction and Interface Morphology between Reversible Metal Anode and Solid Electrolyte in Solid State Batteries. *ACS Appl. Mater. Interfaces* **2022**, *14*, 35545–35554. [CrossRef]
19. Mazur, R.G.; Dickey, D.H. A Spreading Resistance Technique for Resistivity Measurements on Silicon. *J. Electrochem. Soc.* **1966**, *113*, 255–259. [CrossRef]
20. Denhoff, M.W. An accurate calculation of spreading resistance. *J. Phys. D Appl. Phys.* **2006**, *39*, 1761–1765. [CrossRef]
21. Zhang, P.; Lau, Y.Y.; Timsit, R.S. On the Spreading Resistance of Thin-Film Contacts. *IEEE Trans. Electron Devices* **2012**, *59*, 1936–1940. [CrossRef]
22. Eckhardt, J.K.; Fuchs, T.; Burkhardt, S.; Klar, P.J.; Janek, J.; Heiliger, C. 3D Impedance Modeling of Metal Anodes in Solid-State Batteries–Incompatibility of Pore Formation and Constriction Effect in Physical-Based 1D Circuit Models. *ACS Appl. Mater. Interfaces* **2022**, *14*, 42757–42769. [CrossRef] [PubMed]
23. Fleig, J.; Maier, J. Rough electrodes in solid and liquid electrochemistry: Impact of morphology on the impedance. *Solid State Ionics* **1997**, *94*, 199–207. [CrossRef]
24. Jolly, D.S.; Ning, Z.; Darnbrough, J.E.; Kasemchainan, J.; Hartley, G.O.; Adamson, P.; Armstrong, D.E.J.; Marrow, J.; Bruce, P.G. Sodium/Na β″ Alumina Interface: Effect of Pressure on Voids. *ACS Appl. Mater. Interfaces* **2020**, *12*, 678–685. [CrossRef]
25. Koshikawa, H.; Matsuda, S.; Kamiya, K.; Miyayama, M.; Kubo, Y.; Uosaki, K.; Hashimoto, K.; Nakanishi, S. Dynamic changes in charge-transfer resistance at Li metal/$Li_7La_3Zr_2O_{12}$ interfaces during electrochemical Li dissolution/deposition cycles. *J. Power Sources* **2018**, *376*, 147–151. [CrossRef]
26. Bay, M.; Wang, M.; Grissa, R.; Heinz, M.V.F.; Sakamoto, J.; Battaglia, C. Sodium Plating from Na-β″-Alumina Ceramics at Room Temperature, Paving the Way for Fast-Charging All-Solid-State Batteries. *Adv. Energy Mater.* **2020**, *10*, 1902899. [CrossRef]
27. Krauskopf, T.; Hartmann, H.; Zeier, W.G.; Janek, J. Toward a Fundamental Understanding of the Lithium Metal Anode in Solid-State Batteries—An Electrochemo-Mechanical Study on the Garnet-Type Solid Electrolyte $Li_{6.25}Al_{0.25}La_3Zr_2O_{12}$. *ACS Appl. Mater. Interfaces* **2019**, *11*, 14463–14477. [CrossRef]
28. Janek, J. Oscillating reactions at metal electrodes in solid electrolytes. *Solid State Ion.* **1997**, *101–103*, 721–727. [CrossRef]
29. Rohnke, M.; Rosenkranz, C.; Janek, J. The influence of non-equilibrium defects on the anodic dissolution of a metal into a solid electrolyte. *Solid State Ion.* **2006**, *177*, 447–456. [CrossRef]
30. Janek, J.; Majoni, S. Investigation of Charge Transport Across the Ag I AgI-interface: (I) Occurrence of Periodic Phenomena During Anodic Dissolution of Silver. *Ber. Bunsenges. Phys. Chem.* **1995**, *99*, 14–20. [CrossRef]
31. Majoni, S.; Janek, J. Investigation of Charge Transport Across the Agl AgI-Interface: (II) Dilatometric Study of the Anodic Dissolution of Silver. *Ber. Bunsenges. Phys. Chem.* **1998**, *102*, 756–762. [CrossRef]
32. Motoyama, M.; Ejiri, M.; Iriyama, Y. Modeling the Nucleation and Growth of Li at Metal Current Collector/LiPON Interfaces. *J. Electrochem. Soc.* **2015**, *162*, A7067–A7071. [CrossRef]
33. Motoyama, M.; Ejiri, M.; Yamamoto, T.; Iriyama, Y. In Situ Scanning Electron Microscope Observations of Li Plating/Stripping Reactions with Pt Current Collectors on LiPON Electrolyte. *J. Electrochem. Soc.* **2018**, *165*, A1338–A1347. [CrossRef]
34. Motoyama, M.; Hirota, M.; Yamamoto, T.; Iriyama, Y. Temperature Effects on Li Nucleation at Cu/LiPON Interfaces. *ACS Appl. Mater. Interfaces* **2020**, *12*, 38045–38053. [CrossRef]
35. Kazyak, E.; Wang, M.J.; Lee, K.; Yadavalli, S.; Sanchez, A.J.; Thouless, M.D.; Sakamoto, J.; Dasgupta, N.P. Understanding the electro-chemo-mechanics of Li plating in anode-free solid-state batteries with operando 3D microscopy. *Matter* **2022**, *5*, 3912–3934. [CrossRef]
36. Fuchs, T.; Ortmann, T.; Becker, J.; Haslam, C.G.; Ziegler, M.; Singh, V.K.; Rohnke, M.; Mogwitz, B.; Peppler, K.; Nazar, L.F.; et al. Imaging the microstructure of lithium and sodium metal in anode-free solid-state batteries using electron backscatter diffraction. *Nat. Mater.* **2024**, *23*, 1678–1685. [CrossRef]
37. Ortmann, T.; Fuchs, T.; Eckhardt, J.K.; Ding, Z.; Ma, Q.; Tietz, F.; Kübel, C.; Rohnke, M.; Janek, J. Deposition of Sodium Metal at the Copper-NaSICON Interface for Reservoir-Free Solid-State Sodium Batteries. *Adv. Energy Mater.* **2024**, *14*, 2302729. [CrossRef]
38. Ortmann, T.; Burkhardt, S.; Eckhardt, J.K.; Fuchs, T.; Ding, Z.; Sann, J.; Rohnke, M.; Ma, Q.; Tietz, F.; Fattakhova-Rohlfing, D.; et al. Kinetics and Pore Formation of the Sodium Metal Anode on NASICON-Type $Na_{3.4}Zr_2Si_{2.4}P_{0.6}O_{12}$ for Sodium Solid-State Batteries. *Adv. Energy Mater.* **2023**, *13*, 2202712. [CrossRef]

39. Gao, H.; Xin, S.; Xue, L.; Goodenough, J.B. Stabilizing a High-Energy-Density Rechargeable Sodium Battery with a Solid Electrolyte. *Chem* **2018**, *4*, 833–844. [CrossRef]
40. Oh, J.A.S.; Wang, Y.; Zeng, Q.; Sun, J.; Sun, Q.; Goh, M.; Chua, B.; Zeng, K.; Lu, L. Intrinsic low sodium/NASICON interfacial resistance paving the way for room temperature sodium-metal battery. *J. Colloid Interface Sci.* **2021**, *601*, 418–426. [CrossRef]
41. Quérel, E.; Seymour, I.D.; Cavallaro, A.; Ma, Q.; Tietz, F.; Aguadero, A. The role of NaSICON surface chemistry in stabilizing fast-charging Na metal solid-state batteries. *J. Phys. Energy* **2021**, *3*, 044007. [CrossRef]
42. Quérel, E.; Williams, N.J.; Seymour, I.D.; Skinner, S.J.; Aguadero, A. Operando Characterization and Theoretical Modeling of Metal | Electrolyte Interphase Growth Kinetics in Solid-State Batteries. Part I: Experiments. *Chem. Mater.* **2023**, *35*, 853–862. [CrossRef] [PubMed]
43. Lu, Y.; Li, L.; Zhang, Q.; Niu, Z.; Chen, J. Electrolyte and Interface Engineering for Solid-State Sodium Batteries. *Joule* **2018**, *2*, 1747–1770. [CrossRef]
44. Tang, X.; Han, W.; Zhang, Y.; Liu, S. Interface engineering of sodium metal anode for all-solid-state sodium batteries. *J. Power Sources* **2024**, *623*, 235397. [CrossRef]
45. Tsai, C.; Lan, T.; Dellen, C.; Ling, Y.; Ma, Q.; Fattakhova-Rohlfing, D.; Guillon, O.; Tietz, F. Dendrite-tolerant all-solid-state sodium batteries and an important mechanism of metal self-diffusion. *J. Power Sources* **2020**, *476*, 228666. [CrossRef]
46. Li, R.; Jiang, D.; Du, P.; Yuan, C.; Cui, X.; Tang, Q.; Zheng, J.; Li, Y.; Lu, K.; Ren, X.; et al. Negating Na||$Na_3Zr_2Si_2PO_{12}$ interfacial resistance for dendrite-free and "Na-less" solid-state batteries. *Chem. Sci.* **2022**, *13*, 14132–14140. [CrossRef]
47. Pei, A.; Zheng, G.; Shi, F.; Li, Y.; Cui, Y. Nanoscale Nucleation and Growth of Electrodeposited Lithium Metal. *Nano Lett.* **2017**, *17*, 1132–1139. [CrossRef]
48. Xu, P.; Li, X.; Yan, M.; Ni, H.; Huang, H.; Lin, X.; Liu, X.; Fan, J.; Zheng, M.; Yuan, R.; et al. A highly reversible sodium metal anode by mitigating electrodeposition overpotential. *J. Mater. Chem. A* **2021**, *9*, 22892–22900. [CrossRef]
49. Willow, A.; Hussein, H.E.M.; Vajirakaphan, S.; Chasri, A.; Margadonna, S. Improving In-Situ Sodium Metal Plating on Copper Foil Through Optimization of Mechanical Pressure: Towards High-Performance Anode-Free Sodium Ion Batteries. *Front. Energy Res.* **2022**, *10*, 888321. [CrossRef]
50. Sayahpour, B.; Li, W.; Bai, S.; Lu, B.; Han, B.; Chen, Y.; Deysher, G.; Parab, S.; Ridley, P.; Raghavendran, G.; et al. Quantitative analysis of sodium metal deposition and interphase in Na metal batteries. *Energy Environ. Sci.* **2024**, *17*, 1216–1228. [CrossRef]
51. Louli, A.J.; Genovese, M.; Weber, R.; Hames, S.G.; Logan, E.R.; Dahn, J.R. Exploring the Impact of Mechanical Pressure on the Performance of Anode-Free Lithium Metal Cells. *J. Electrochem. Soc.* **2019**, *166*, A1291–A1299. [CrossRef]
52. Zhang, X.; Wang, Q.J.; Harrison, K.L.; Roberts, S.A.; Harris, S.J. Pressure-Driven Interface Evolution in Solid-State Lithium Metal Batteries. *Cell Rep. Phys. Sci.* **2020**, *1*, 100012. [CrossRef]
53. Wang, M.J.; Chang, J.; Wolfenstine, J.B.; Sakamoto, J. Analysis of elastic, plastic, and creep properties of sodium metal and implications for solid-state batteries. *Materialia* **2020**, *12*, 100792. [CrossRef]
54. Sun, C.; Li, Y.; Sun, Z.; Yuan, X.; Jin, H.; Zhao, Y. Ferroelectric interface for efficient sodium metal cycling in anode-free solid-state batteries. *Mater. Today* **2024**, *80*, 395–405. [CrossRef]
55. Ding, Z.; Tang, Y.; Ortmann, T.; Eckhardt, J.K.; Dai, Y.; Rohnke, M.; Melinte, G.; Heiliger, C.; Janek, J.; Kübel, C. The Impact of Microstructure on Filament Growth at the Sodium Metal Anode in All-Solid-State Sodium Batteries. *Adv. Energy Mater.* **2023**, *13*, 2302322. [CrossRef]
56. Ding, Z.; Tang, Y.; Ortmann, T.; Eckhardt, J.K.; Rohnke, M.; Melinte, G.; Heiliger, C.; Janek, J.; Kübel, C. Microstructural Influence on Sodium Filament Growth in All Solid-state Batteries. *BIO Web Conf.* **2024**, *129*, 25020. [CrossRef]
57. Lou, S.; Zhang, F.; Fu, C.; Chen, M.; Ma, Y.; Yin, G.; Wang, J. Interface Issues and Challenges in All-Solid-State Batteries: Lithium, Sodium, and Beyond. *Adv. Mater.* **2020**, *32*, 2000721. [CrossRef]
58. Tian, Y.; Shi, T.; Richards, W.D.; Li, J.; Kim, J.C.; Bo, S.; Ceder, G. Compatibility issues between electrodes and electrolytes in solid-state batteries. *Energy Environ. Sci.* **2017**, *10*, 1150–1166. [CrossRef]
59. Wang, S.; Xu, H.; Li, W.; Dolocan, A.; Manthiram, A. Interfacial Chemistry in Solid-state Batteries: Formation of Inter-phase and Its Consequences. *J. Am. Chem. Soc.* **2018**, *140*, 250–257. [CrossRef]
60. Ma, Q.; Ortmann, T.; Yang, A.; Sebold, D.; Burkhardt, S.; Rohnke, M.; Tietz, F.; Fattakhova-Rohlfing, D.; Janek, J.; Guillon, O. Enhancing the Dendrite Tolerance of NaSICON Electrolytes by Suppressing Edge Growth of Na Electrode along Ceramic Surface. *Adv. Energy Mater.* **2022**, *12*, 2201680. [CrossRef]
61. Wang, X.; Chen, J.; Mao, Z.; Wang, D. Effective resistance to dendrite growth of NASICON solid electrolyte with lower electronic conductivity. *Chem. Eng. J.* **2022**, *427*, 130899. [CrossRef]
62. Zhang, Z.; Wenzel, S.; Zhu, Y.; Sann, J.; Shen, L.; Yang, J.; Yao, X.; Hu, Y.; Wolverton, C.; Li, H.; et al. $Na_3Zr_2Si_2PO_{12}$: A Stable Na^+-Ion Solid Electrolyte for Solid-State Batteries. *ACS Appl. Energy Mater.* **2020**, *3*, 7427–7437. [CrossRef]
63. Hu, X.; Wang, M.; Liu, Y.; Meng, X.; Zhong, Y.; Wang, X.; Tu, J. Fluorinated solid electrolyte interphase enables interfacial stability for sulfide-based solid-state sodium metal batteries. *Chem. Eng. J.* **2024**, *499*, 156290. [CrossRef]

64. Gao, Z.; Yang, J.; Yuan, H.; Fu, H.; Li, Y.; Li, Y.; Ferber, T.; Guhl, C.; Sun, H.; Jaegermann, W.; et al. Stabilizing $Na_3Zr_2Si_2PO_{12}$/Na Interfacial Performance by Introducing a Clean and Na-Deficient Surface. *Chem. Mater.* **2020**, *32*, 3970–3979. [CrossRef]
65. Li, Y.; Sun, C.; Sun, Z.; Li, M.; Jin, H.; Zhao, Y. Boosting Na-O Affinity in $Na_3Zr_2Si_2PO_{12}$ Electrolyte Promises Highly Rechargeable Solid-State Sodium Batteries. *Adv. Funct. Mater.* **2024**, *34*, 2403937. [CrossRef]
66. Wang, C.; Jin, H.; Zhao, Y. Surface Potential Regulation Realizing Stable Sodium/$Na_3Zr_2Si_2PO_{12}$ Interface for Room-Temperature Sodium Metal Batteries. *Small* **2021**, *17*, 2100974. [CrossRef]
67. Zhou, W.; Li, Y.; Xin, S.; Goodenough, J.B. Rechargeable Sodium All-Solid-State Battery. *ACS Cent. Sci.* **2017**, *3*, 52–57. [CrossRef]
68. Lu, Y.; Alonso, J.A.; Yi, Q.; Lu, L.; Wang, Z.L.; Sun, C. A High-Performance Monolithic Solid-State Sodium Battery with Ca^{2+} Doped $Na_3Zr_2Si_2PO_{12}$ Electrolyte. *Adv. Energy Mater.* **2019**, *9*, 1901205. [CrossRef]
69. Tian, H.; Liu, S.; Deng, L.; Wang, L.; Dai, L. New-type Hf-based NASICON electrolyte for solid-state Na-ion batteries with superior long-cycling stability and rate capability. *Energy Storage Mater.* **2021**, *39*, 232–238. [CrossRef]
70. Suo, J.; Zhao, Q.; Tian, H.; Wang, L.; Dai, L.; Luo, J.; Liu, S. Designing a quasi-liquid alloy interface for solid Na-ion battery. *ACS Nano* **2023**, *17*, 10229–10235. [CrossRef]
71. Miao, X.; Di, H.; Ge, X.; Zhao, D.; Wang, P.; Wang, R.; Wang, C.; Yin, L. AlF_3-modified anode-electrolyte interface for effective Na dendrites restriction in NASICON-based solid-state electrolyte. *Energy Storage Mater.* **2020**, *30*, 170–178. [CrossRef]
72. Yu, X.; Manthiram, A. Sodium-Sulfur Batteries with a Polymer-Coated NASICON-type Sodium-Ion Solid Electrolyte. *Matter* **2019**, *1*, 439–451. [CrossRef]
73. Miao, X.; Wang, H.; Sun, R.; Ge, X.; Zhao, D.; Peng Wang, P.; Wang, R.; Yin, L. Isotropous Sulfurized Polyacrylonitrile Interlayer with Homogeneous Na^+ Flux Dynamics for Solid-State Na Metal Batteries. *Adv. Energy Mater.* **2021**, *11*, 2003469. [CrossRef]
74. Chi, X.; Hao, F.; Zhang, J.; Wu, X.; Zhang, Y.; Gheytani, S.; Wen, Z.; Yao, Y. A high-energy quinone-based all-solid-state sodium metal battery. *Nano Energy* **2019**, *62*, 718–724. [CrossRef]
75. Yang, J.; Gao, Z.; Ferber, T.; Zhang, H.; Guhl, C.; Yang, L.; Li, Y.; Deng, Z.; Liu, P.; Cheng, C.; et al. Guided-formation of favorable interface for stabilizing Na metal solid-state batteries. *J. Mater. Chem. A* **2020**, *8*, 7828–7835. [CrossRef]
76. Wu, T.; Wen, Z.; Sun, C.; Wu, X.; Zhang, S.; Yang, J. Disordered Carbon Tubes Based on Cotton Cloth for Modulating the Interface Impedance in β″-Al_2O_3-based Solid-state Sodium Metal Batteries. *J. Mater. Chem. A* **2018**, *6*, 12623–12629. [CrossRef]
77. Matios, E.; Wang, H.; Wang, C.; Hu, X.; Lu, X.; Luo, J.; Li, W. Graphene Regulated Ceramic Electrolyte for Solid-State Sodium Metal Battery with Superior Electrochemical Stability. *ACS Appl. Mater. Interfaces* **2019**, *11*, 5064–5072. [CrossRef] [PubMed]
78. Fang, D.; Li, Y.; Wang, C.; Miao, R.; Yang, S.; Zhao, Y.; Ding, Y.; He, J.; Chen, L.; Li, N.; et al. Wide-temperature solid-state sodium metal batteries using Na^+ superionic conductor-type solid electrolytes. *Energy Storage Mater.* **2025**, *74*, 103973. [CrossRef]
79. Jaschin, P.W.; Tang, C.R.; Eric, D.; Wachsman, E.D. High-rate cycling in 3D dual-doped NASICON architectures toward room-temperature sodium-metal-anode solid-state batteries. *Energy Environ. Sci.* **2024**, *17*, 727–737. [CrossRef]
80. Wang, X.; Chen, J.; Wang, D.; Mao, Z. Improving the alkali metal electrode/inorganic solid electrolyte contact via room-temperature ultrasound solid welding. *Nat. Commun.* **2021**, *12*, 7109. [CrossRef]
81. Uchida, Y.; Hasegawa, G.; Shima, K.; Inada, M.; Enomoto, N.; Akamatsu, H.; Hayashi, K. Insights into Sodium Ion Transfer at the Na/NASICON Interface Improved by Uniaxial Compression. *ACS Appl. Energy Mater.* **2019**, *2*, 2913–2920. [CrossRef]
82. Chowdhury, S.; Mahato, J.C.; Chung, J.S.; Kang, S.G.; Gupta, B.C. Theoretical prediction of the potential of using two-dimensional V_2S_2 as an effective anode for alkali metal ion batteries. *Surf. Interfaces* **2024**, *51*, 104750. [CrossRef]
83. Dey, T.; Chowdhury, S.; Kang, S.G.; Sen, P.; Gupta, B.C.; Mahato, J.C. Two-dimensional $ScTe_2$ monolayer: An efficient anode material for sodium-ion battery and cathode material for lithium-ion and potassium-ion battery. *Comput. Mater. Sci.* **2025**, *253*, 113824. [CrossRef]
84. Gao, H.; Xue, L.; Xin, S.; Park, K.; Goodenough, J.B. A Plastic–Crystal Electrolyte Interphase for All-Solid-State Sodium Batteries. *Angew. Chem. Int. Ed.* **2017**, *56*, 5541–5545. [CrossRef]
85. Zhang, Z.; Zhang, Q.; Shi, J.; Chu, Y.S.; Yu, X.; Xu, K.; Ge, M.; Yan, H.; Li, W.; Gu, L.; et al. A Self-Forming Composite Electrolyte for Solid-State Sodium Battery with Ultralong Cycle Life. *Adv. Energy Mater.* **2016**, *6*, 1601196. [CrossRef]
86. Wang, Q.; Yu, C.; Li, L.; Liu, X.; Zhang, X.; Gao, G.; Wang, Y.; Li, G. Sc-doping in $Na_3Zr_2Si_2PO_{12}$ electrolytes enables preeminent performance of solid-state sodium batteries in a wide temperature range. *Energy Storage Mater.* **2023**, *54*, 135–145. [CrossRef]
87. Zatovsky, I.V. NASICON-type $Na_3V_2(PO_4)_3$. *Acta Cryst.* **2010**, *66*, i12. [CrossRef]
88. Zhang, Z.; Zhang, Q.; Ren, C.; Luo, F.; Ma, Q.; Hu, Y.; Zhou, Z.; Li, H.; Huang, X.; Chen, L. A ceramic/polymer composite solid electrolyte for sodium batteries. *J. Mater. Chem. A* **2016**, *4*, 15823–15828. [CrossRef]
89. Pandit, B.; Johansen, M.; Martínez-Cisneros, C.S.; Naranjo-Balseca, J.M.; Levenfeld, B.; Ravnsbæk, D.B.; Varez, A. $Na_3V_2(PO_4)_3$ Cathode for Room-Temperature Solid-State Sodium-Ion Batteries: Advanced In Situ Synchrotron X-ray Studies to Understand Intermediate Phase Evolution. *Chem. Mater.* **2024**, *36*, 2314–2324. [CrossRef]
90. Kehne, P.; Guhl, C.; Mac, Q.; Tietz, F.; Alff, L.; Hausbrand, R.; Komissinskiy, P. Sc-substituted Nasicon solid electrolyte for an all-solid-state Na_xCoO_2/Nasicon/Na sodium model battery with stable electrochemical performance. *J. Power Sources* **2019**, *409*, 86–93. [CrossRef]

91. Li, L.; Yao, J.; Xu, R.; Lin, Q.; Yan, X.; Yu, C.; Zhang, L. Highly stable and encapsulation-microstructural cathode derived by self-pressurization behavior in Na-halides-based all-solid-state batteries. *Energy Storage Mater.* **2023**, *63*, 103016. [CrossRef]
92. Sun, C.; Xie, L.; Wang, B.; Tan, H.; Zhang, Q.; Han, L.; Liu, Y.; Sydorov, D. Improve the cycling performance of solid-state sodium batteries through the design of a cathode interface buffering layer. *Appl. Surf. Sci.* **2025**, *680*, 161265. [CrossRef]
93. Liu, L.; Qi, X.; Ma, Q.; Rong, X.; Hu, Y.; Zhou, Z.; Li, H.; Huang, X.; Chen, L. Toothpaste-like Electrode: A Novel Approach to Optimize the Interface for Solid-State Sodium-Ion Batteries with Ultralong Cycle Life. *ACS Appl. Mater. Interfaces* **2016**, *8*, 32631–32636. [CrossRef] [PubMed]
94. Liang, B.; Lv, Y.; Wang, H.; Li, B.; Zhao, S.; Zheng, L.; Huang, Y.; Hong, Z. Durable high voltage solid-state sodium batteries with Pseudocapacitive P2 layered oxide cathode. *Energy Storage Mater.* **2024**, *73*, 103804. [CrossRef]
95. Yang, S.; Shao, C.; Xiao, X.; Fang, D.; Li, N.; Zhao, E.; Wang, C.; Chen, L.; Li, N.; Li, J.; et al. Revealing stable organic cathode/solid electrolyte interface to promote all-solid-state sodium batteries using organic cathodes. *Energy Storage Mater.* **2024**, *73*, 103857. [CrossRef]
96. Du, K.; Guo, H.; Hu, G.; Peng, Z.; Cao, Y. $Na_3V_2(PO_4)_3$ as cathode material for hybrid lithium ion batteries. *J. Power Sources* **2013**, *223*, 284–288. [CrossRef]
97. Zhu, X.; Zhao, R.; Deng, W.; Ai, X.; Yang, H.; Cao, Y. An All-solid-state and All-organic Sodium-ion Battery based on Redox-active Polymers and Plastic Crystal Electrolyte. *Electrochim. Acta* **2015**, *178*, 55–59. [CrossRef]
98. Ma, Q.; Tietz, F. Solid-State Electrolyte Materials for Sodium Batteries: Towards Practical Applications. *ChemElectroChem* **2020**, *7*, 2693–2713. [CrossRef]
99. Åvall, G.; Mindemark, J.; Brandell, D.; Johansson, P. Sodium-Ion Battery Electrolytes: Modeling and Simulations. *Adv. Energy Mater.* **2018**, *8*, 1703036. [CrossRef]
100. Kim, J.; Yoon, K.; Park, I.; Kang, K. Progress in the Development of Sodium-Ion Solid Electrolytes. *Small Methods* **2017**, *1*, 1700219. [CrossRef]
101. Zhang, Z.; Shao, Y.; Lotsch, B.; Hu, Y.; Li, H.; Janek, J.; Nazar, L.F.; Nan, C.; Maier, J.; Armand, M.; et al. New Horizons for Inorganic Solid State Ion Conductors. *Energy Environ. Sci.* **2018**, *11*, 1945–1976. [CrossRef]
102. Zhao, Q.; Stalin, S.; Zhao, C.; Archer, L.A. Designing solid-state electrolytes for safe, energy-dense batteries. *Nat. Rev. Mater.* **2020**, *5*, 229–252. [CrossRef]
103. Ahmad, H.; Kubra, K.T.; Butt, A.; Nisar, U.; Iftikhar, F.J.; Ali, G. Recent progress, challenges, and perspectives in the development of solid-state electrolytes for sodium batteries. *J. Power Sources* **2023**, *581*, 233518. [CrossRef]
104. Hou, W.; Guo, X.; Shen, X.; Amine, K.; Yu, H.; Lu, J. Solid electrolytes and interfaces in all-solid-state sodium batteries: Progress and perspective. *Nano Energy* **2018**, *52*, 279–291. [CrossRef]
105. Kumar, P.P.; Yashonath, S. Ionic conduction in the solid state. *J. Chem. Sci.* **2006**, *118*, 135–154. [CrossRef]
106. Guin, M.; Tietz, F. Survey of the transport properties of sodium superionic conductor materials for use in sodium batteries. *J. Power Sources* **2015**, *273*, 1056–1064. [CrossRef]
107. Wu, J.; Zhang, R.; Fu, Q.; Zhang, J.; Zhou, X.; Gao, P.; Xu, C.; Liu, J.; Guo, X. Inorganic Solid Electrolytes for All-Solid-State Sodium Batteries: Fundamentals and Strategies for Battery Optimization. *Adv. Funct. Mater.* **2021**, *31*, 2008165. [CrossRef]
108. Yang, Z.; Tang, B.; Ren, D.; Yu, X.; Gao, Y.; Wu, Y.; Yang, Y.; Chen, Z.; Zhou, Z. Advancing solid-state sodium batteries: Status quo of sulfide-based solid electrolytes. *Mater. Today* **2024**, *80*, 429–449. [CrossRef]
109. Goodenough, J.B.; Hong, H.Y.; Kafalas, J.A. Fast Na^+-ion transport in skeleton structures. *Mater. Res. Bull.* **1976**, *11*, 203–220. [CrossRef]
110. Hong, H.Y. Crystal structures and crystal chemistry in the system $Na_{1+x}Zr_2Si_xP_{3-x}O_{12}$. *Mater. Res. Bull.* **1976**, *11*, 173–182. [CrossRef]
111. Boilot, J.P.; Collin, G.; Colomban, P. Relation structure-fast ion conduction in the NASICON solid solution. *J. Solid State Chem.* **1998**, *73*, 160–171. [CrossRef]
112. Park, H.; Jung, K.; Nezafati, M.; Kim, C.; Kang, B. Sodium Ion Diffusion in Nasicon ($Na_3Zr_2Si_2PO_{12}$) Solid Electrolytes: Effects of Excess Sodium. *ACS Appl. Mater. Interfaces* **2016**, *8*, 27814–27824. [CrossRef]
113. Zhang, Z.; Zou, Z.; Kaup, K.; Xiao, R.; Shi, S.; Avdeev, M.; Hu, Y.; Wang, D.; He, B.; Li, H.; et al. Correlated Migration Invokes Higher Na+-Ion Conductivity in NaSICON-Type Solid Electrolytes. *Adv. Energy Mater.* **2019**, *9*, 1902373. [CrossRef]
114. Ma, Q.; Tsai, C.; Wei, X.; Heggen, M.; Tietz, F.; Irvine, J.T.S. Room temperature demonstration of a sodium superionic conductor with grain conductivity in excess of 0.01 S cm-1 and its primary applications in symmetric battery cells. *J. Mater. Chem. A* **2019**, *7*, 7766–7776. [CrossRef]
115. Fuentes, R.O.; Figueiredo, F.; Marques, F.M.B.; Franco, J.I. Optimised NASICON Ceramics for Na^+ Sensing. *Ionics* **2002**, *8*, 383–390. [CrossRef]
116. He, J.; Yang, S.; Xiao, X.; Fang, D.; Miao, R.; Wang, C.; Chen, L.; Li, N.; Li, J.; Su, Y.; et al. Aliovalent cation substitution in $Na_3Zr_2Si_2PO_{12}$ for practical solid-state sodium metal batteries. *Energy Storage Mater.* **2025**, *75*, 104037. [CrossRef]

117. Takahashi, T.; Kuwabara, K.; Shibata, M. Solid-state Ionics—Conductivities of Na^+ ion conductors based on NASICON. *Solid State Ion.* **1980**, *1*, 163–175. [CrossRef]
118. Bohnke, O.; Ronchetti, S.; Mazza, D. Conductivity measurements on nasicon and nasicon-modified materials. *Solid State Ion.* **1999**, *122*, 127–136. [CrossRef]
119. Anantharamulu, N.; Rao, K.K.; Rambabu, G.; Kumar, B.V.; Radha, V.; Vithal, M. A wide-ranging review on Nasicon type materials. *J. Mater. Sci.* **2011**, *46*, 2821–2837. [CrossRef]
120. Chen, D.; Luo, F.; Zhou, W.; Zhu, D. Influence of Nb^{5+}, Ti^{4+}, Y^{3+} and Zn^{2+} doped $Na_3Zr_2Si_2PO_{12}$ solid electrolyte on its conductivity. *J. Alloys Compd.* **2018**, *757*, 348–355. [CrossRef]
121. Yang, J.; Liu, G.; Avdeev, M.; Wan, H.; Han, F.; Shen, L.; Zou, Z.; Shi, S.; Hu, Y.; Wang, C.; et al. Ultrastable All-Solid-State Sodium Rechargeable Batteries. *ACS Energy Lett.* **2020**, *5*, 2835–2841. [CrossRef]
122. Vogel, E.M.; Cava, R.J.; Rietman, E. Na+ ion conductivity and crystallographic cell characterization in the Hf-nasicon system $Na_{1+x}Hf_2Si_xP_{3-x}O_{12}$. *Solid State Ion.* **1984**, *14*, 1–6. [CrossRef]
123. Bogusz, W.; Krok, F.; Jakubowski, W. Influence of doping on some physical properties of NASICON. *Solid State Ion.* **1983**, *9–10*, 803–807. [CrossRef]
124. Krok, F.; Kony, D.; Dygas, J.R.; Jakubowski, W.; Bogusz, W. On some properties of NASICON doped with MgO and CoO. *Solid State Ion.* **1989**, *36*, 251–254. [CrossRef]
125. Ma, Q.; Guin, M.; Naqash, S.; Tsai, C.; Tietz, F.; Guillon, O. Scandium-Substituted $Na_3Zr_2(SiO_4)_2(PO_4)$ Prepared by a Solution-Assisted Solid-State Reaction Method as Sodium-Ion Conductors. *Chem. Mater.* **2016**, *28*, 4821–4828. [CrossRef]
126. Yang, J.; Wan, H.; Zhang, Z.; Liu, G.; Xu, X.; Hu, Y.; Yao, X. NASICON-structured $Na_{3.1}Zr_{1.95}Mg_{0.05}Si_2PO_{12}$ solid electrolyte for solid-state sodium batteries. *Rare Met.* **2018**, *37*, 480–487. [CrossRef]
127. Oh, J.A.S.; He, L.; Plewa, A.; Morita, M.; Zhao, Y.; Sakamoto, T.; Song, X.; Zhai, W.; Zeng, K.; Lu, L. Composite NASICON ($Na_3Zr_2Si_2PO_{12}$) Solid-State Electrolyte with Enhanced Na^+ Ionic Conductivity: Effect of Liquid Phase Sintering. *ACS Appl. Mater. Interfaces* **2019**, *11*, 40125–40133. [CrossRef]
128. Nafis, M.S.; Liang, Z.; Lee, S.; Ban, C. Structural engineering developments in sulfide solid-state electrolytes for lithium and sodium solid-state batteries. *Nano Energy* **2025**, *133*, 110447. [CrossRef]
129. Hayashi, A.; Noi, K.; Tanibata, N.; Nagao, M.; Tatsumisago, M. High sodium ion conductivity of glasseceramic electrolytes with cubic Na_3PS_4. *J. Power Sources* **2014**, *258*, 420–423. [CrossRef]
130. Zhang, L.; Zhang, D.; Yang, K.; Yan, X.; Wang, L.; Mi, J.; Xu, B.; Li, Y. Vacancy-Contained Tetragonal Na_3SbS_4 Superionic Conductor. *Adv. Sci.* **2016**, *3*, 1600089. [CrossRef]
131. Zhang, D.; Cao, X.; Xu, D.; Wang, N.; Yu, C.; Hu, W.; Yan, X.; Mi, J.; Wen, B.; Wang, L.; et al. Synthesis of cubic Na_3SbS_4 solid electrolyte with enhanced ion transport for all-solid-state sodium-ion batteries. *Electrochim. Acta* **2018**, *259*, 100–109. [CrossRef]
132. Zhang, Z.; Ramos, E.; Lalère, F.; Assoud, J.; Kaup, K.; Hartman, P.; Nazar, L.F. $Na_{11}Sn_2PS_{12}$: A New Solid State Sodium Superionic Conductor. *Energy Environ. Sci.* **2018**, *11*, 87–93. [CrossRef]
133. Hayashi, A.; Noi, K.; Sakuda, A.; Tatsumisago, M. Superionic glass-ceramic electrolytes for room-temperature rechargeable sodium batteries. *Nat. Commun.* **2012**, *3*, 856. [CrossRef]
134. Banerjee, A.; Park, K.H.; Heo, J.W.; Nam, Y.J.; Moon, C.K.; Oh, S.M.; Seung-Tae Hong, S.; Jung, Y.S. Na_3SbS_4: A Solution Processable Sodium Superionic Conductor for All-Solid-State Sodium-Ion Batteries. *Angew. Chem. Int. Ed.* **2016**, *55*, 9634–9638. [CrossRef]
135. Noi, K.; Hayashi, A.; Tatsumisago, M. Structure and properties of the Na_2S–P_2S_5 glasses and glass—ceramics prepared by mechanical milling. *J. Power Sources* **2014**, *269*, 260–265. [CrossRef]
136. Wang, H.; Chen, Y.; Hood, Z.D.; Sahu, G.; Pandian, A.S.; Keum, J.K.; An, K.; Liang, C. An Air-Stable Na_3SbS_4 Superionic Conductor Prepared by a Rapid and Economic Synthetic Procedure. *Angew. Chem. Int. Ed.* **2016**, *55*, 8551–8555. [CrossRef] [PubMed]
137. Kim, S.K.; Mao, A.; Sen, S.; Kim, S. Fast Na-Ion Conduction in a Chalcogenide Glass–Ceramic in the Ternary System Na_2Se–Ga_2Se_3–$GeSe_2$. *Chem. Mater.* **2014**, *26*, 5695–5699. [CrossRef]
138. Jansen, M.; Henseler, U. Synthesis, structure determination, and ionic conductivity of sodium tetrathiophosphate. *J. Solid State Chem.* **1992**, *99*, 110–119. [CrossRef]
139. Tatsumisago, M.; Hayashi, A. Sulfide Glass-Ceramic Electrolytes for All-Solid-State Lithium and Sodium Batteries. *Int. J. Appl. Glass Sci.* **2014**, *5*, 226–235. [CrossRef]
140. Chu, I.; Kompella, C.S.; Nguyen, H.; Zhu, Z.; Hy, S.; Deng, Z.; Meng, Y.S.; Ong, S.P. Room-Temperature All-solid-state Rechargeable Sodium-ion Batteries with a Cl-doped Na_3PS_4 Superionic Conductor. *Sci. Rep.* **2016**, *6*, 33733. [CrossRef]
141. de Klerk, N.J.J.; Wagemaker, M. Diffusion Mechanism of the Sodium-Ion Solid Electrolyte Na3PS4 and Potential Improvements of Halogen Doping. *Chem. Mater.* **2016**, *28*, 3122–3130. [CrossRef]
142. Bo, S.; Wang, Y.; Kim, J.C.; Richards, W.D.; Ceder, G. Computational and Experimental Investigations of Na-Ion Conduction in Cubic Na_3PSe_4. *Chem. Mater.* **2016**, *28*, 252–258. [CrossRef]

143. Tanibata, N.; Noi, K.; Hayashi, A.; Tatsumisago, M. Preparation and characterization of highly sodium ion conducting Na_3PS_4–Na_4SiS_4 solid electrolytes. *RSC Adv.* **2014**, *4*, 17120–17123. [CrossRef]
144. Zhang, L.; Yang, K.; Mi, J.; Lu, L.; Zhao, L.; Wang, L.; Li, Y.; Zeng, H. Na_3PSe_4; A Novel Chalcogenide Solid Electrolyte with High Ionic Conductivity. *Adv. Energy Mater.* **2015**, *5*, 1501294. [CrossRef]
145. Zhu, Z.; Chu, I.; Deng, Z.; Ong, S.P. Role of Na^+ Interstitials and Dopants in Enhancing the Na^+ Conductivity of the Cubic Na_3PS_4 Superionic Conductor. *Chem. Mater.* **2015**, *27*, 8318–8325. [CrossRef]
146. Yu, L.; Jiao, Q.; Liang, B.; Shan, H.; Lin, C.; Gao, C.; Shen, X.; Dai, S. Exceptionally high sodium ion conductivity and enhanced air stability in Na_3SbS_4 via germanium doping. *J. Alloys and Compd.* **2022**, *913*, 165229. [CrossRef]
147. Yu, Z.; Shang, S.; Seo, J.; Wang, D.; Luo, X.; Huang, Q.; Chen, S.; Lu, J.; Li, X.; Liu, Z.; et al. Exceptionally High Ionic Conductivity in $Na_3P_{0.62}As_{0.38}S_4$ with Improved Moisture Stability for Solid-State Sodium-Ion Batteries. *Adv. Mater.* **2017**, *29*, 1605. [CrossRef]
148. Bo, S.; Wang, Y.; Ceder, G. Structural and Na-ion conduction characteristics of $Na_3PS_xSe_{4-x}$. *J. Mater. Chem. A* **2016**, *4*, 9044–9053. [CrossRef]
149. Takayanagi, T.; Nasu, A.; Tsuji, F.; Sakuda, A.; Tatsumisago, M.; Hayashi, A. Mechanochemically Prepared Highly Conductive $Na_{2.88}Sb_{0.88}W_{0.12}S_4$–NaI Composite Electrolytes for All-Solid-State Sodium Battery. *Electrochemistry* **2022**, *90*, 047005. [CrossRef]
150. Takayanagi, T.; Nasu, A.; Tsuji, F.; Motohashi, K.; Sakuda, A.; Tatsumisago, M.; Hayashi, A. Preparation and characterization of $Na_{2.88}Sb_{0.88}W_{0.12}S_{4-x}O_x$ solid electrolyte. *J. Ceram. Soc. Jpn.* **2022**, *130*, 498–503. [CrossRef]
151. Hayashi, A.; Masuzawa, N.; Yubuchi, S.; Tsuji, F.; Hotehama, C.; Sakuda, A.; Tatsumisago, M. A sodium-ion sulfide solid electrolyte with unprecedented conductivity at room temperature. *Nat. Commun.* **2019**, *10*, 5266. [CrossRef]
152. Hibi, Y.; Tanibata, N.; Hayashi, A.; Tatsumisago, M. Preparation of sodium ion conducting Na_3PS_4–NaI glasses by a mechanochemical technique. *Solid State Ion.* **2015**, *270*, 6–9. [CrossRef]
153. Tsuji, F.; Nasu, A.; Sakuda, A.; Tatsumisago, M.; Hayashi, A. Mechanochemical synthesis and characterization of $Na_{3-x}P_{1-x}W_xS_4$ solid electrolytes. *J. Power Sources* **2021**, *506*, 230100. [CrossRef]
154. Fuchs, T.; Culver, S.P.; Till, P.; Zeier, W.G. Defect-Mediated Conductivity Enhancements in $Na_{3-x}Pn_{1-x}W_xS_4$ (Pn = P, Sb) Using Aliovalent Substitutions. *ACS Energy Lett.* **2020**, *5*, 146–151. [CrossRef]
155. Oh, K.; Chang, D.; Park, I.; Yoon, K.; Kang, K. First-Principles Investigations on Sodium Superionic Conductor $Na_{11}Sn_2PS_{12}$. *Chem. Mater.* **2019**, *31*, 6066–6075. [CrossRef]
156. Richards, W.R.; Tsujimura, T.; Miara, L.J.; Wang, Y.; Kim, J.C.; Ong, S.P.; Uechi, I.; Suzuki, N.; Ceder, G. Design and synthesis of the superionic conductor $Na_{10}SnP_2S_{12}$. *Nat. Commun.* **2016**, *7*, 11009. [CrossRef] [PubMed]
157. Feng, X.; Chien, P.; Zhu, Z.; Chu, I.; Wang, P.; Immediato-Scuotto, M.; Arabzadeh, H.; Ong, S.P.; Hu, Y. Studies of Functional Defects for Fast Na-Ion Conduction in $Na_{3-y}PS_{4-x}Cl_x$ with a Combined Experimental and Computational Approach. *Adv. Funct. Mater.* **2019**, *29*, 1807951. [CrossRef]
158. Yu, L.; Yin, J.; Gao, C.; Lin, C.; Shen, X.; Dai, S.; Jiao, Q. Halogen Doping Mechanism and Interface Strengthening in the Na_3SbS_4 Electrolyte via Solid-State Synthesis. *ACS Appl. Mater. Interfaces* **2023**, *15*, 31635–31642. [CrossRef]
159. Shu, L.; Gao, C.; Liu, Y.; Zhou, X.; Ma, H.; Zhang, X.; Shen, X.; Dai, S.; Lin, C.; Jiao, Q. Enhancing interface stability and ionic conductivity in the designed $Na_3SbP_{0.4x}S_{4-x}O_x$ sulfide solid electrolyte through bridging oxygen. *J. Colloid Interface Sci.* **2023**, *652*, 2042–2053. [CrossRef]
160. Wang, Y.; Richards, W.D.; Bo, S.; Miara, L.J.; Ceder, G. Computational Prediction and Evaluation of Solid-State Sodium Superionic Conductors $Na_7P_3X_{11}$ (X = O, S, Se). *Chem. Mater.* **2017**, *29*, 7475–7482. [CrossRef]
161. Matsuo, M.; Kuromoto, S.; Sato, T.; Oguchi, H.; Takamura, H.; Orimo, S. Sodium ionic conduction in complex hydrides with $[BH_4]^-$ and $[NH_2]^-$ anions. *Appl. Phys. Lett.* **2012**, *100*, 203904. [CrossRef]
162. Udovic, T.J.; Motoaki Matsuo, M.; Unemoto, A.; Verdal, N.; Stavila, V.; Skripov, A.V.; Rush, J.J.; Takamura, H.; Orimo, S. Sodium superionic conduction in $Na_2B_{12}H_{12}$. *Chem. Commun.* **2014**, *50*, 3750–3752. [CrossRef]
163. Zhou, L.; Bazak, J.D.; Singh, B.; Li, C.; Assoud, A.; Washton, N.M.; Murugesan, V.; Nazar, L.F. A New Sodium Thioborate Fast Ion Conductor: $Na_3B_5S_9$. *Angew. Chem. Int. Ed.* **2023**, *62*, e202300404. [CrossRef]
164. Fu, C.; Li, Y.; Xu, W.; Feng, X.; Gu, W.; Liu, J.; Deng, W.; Wang, W.; Abeykoon, A.M.M.; Su, L.; et al. $LaCl_3$-based sodium halide solid electrolytes with high ionic conductivity for all-solid-state batteries. *Nat. Commun.* **2024**, *15*, 4315. [CrossRef]